ELECTROMAGNETIC WAVE SENSOR FOR SEABED LOGGING USING THE FLUXGATE TECHNOLOGY

YUSUMUZI EMMANUEL DLAMINI

ELECTRICAL & ELECTRONICS ENGINEERING
UNIVERSITI TEKNOLOGI PETRONAS
JUNE 2010

ELECTROMAGNETIC WAVE SENSOR FOR SEABED LOGGING USING THE FLUXGATE TECHNOLOGY

By

VUSUMUZI EMMANUEL DLAMINI

FINAL PROJECT REPORT

Submitted to the Electrical & Electronics Engineering Programme
in Partial Fulfillment of the Requirements
for the Degree
Bachelor of Engineering (Hons)
(Electrical & Electronics Engineering)

Universiti Teknologi Petronas
Bandar Seri Iskandar
31750 Tronoh
Perak Darul Ridzuan

CERTIFICATION OF APPROVAL

ELECTROMAGNETIC WAVE SENSOR FOR SEABED LOGGING USING THE FLUXGATE TECHNOLOGY

By

Vusumuzi Emmanuel Dlamini

A project dissertation submitted to the
Electrical & Electronics Engineering Programme
Universiti Teknologi PETRONAS
in partial fulfillment of the requirement for the
Bachelor of Engineering (Hons)
(Electrical & Electronics Engineering)

Approved:

_____

Associate Professor Dr. Noorhana binti Yahya
Project Supervisor

UNIVERSITI TEKNOLOGI PETRONAS
TRONOH, PERAK

June 2010

CERTIFICATION OF ORIGINALITY

This is to certify that I am responsible for the work submitted in this project, that the original work is my own except as specified in the references and acknowledgements, and that the original work contained herein have not been undertaken or done by unspecified sources or persons.

Vusumuzi Emmanuel Dlamini

ABSTRACT

Designing and manufacturing detectors used for deepwater oil and gas exploration can be very challenging. Detectors used for this purpose; need to have great accuracy and reliability in detecting extremely low frequency EM signals (as low as 1 kHz). Often these Electromagnetic (EM) waves to be detected have a diminished capacity (poor signal to noise ratio/ SNR) due to the very long depth (more than 2500m) they travel beneath the seafloor to reach the potential hydrocarbon reservoirs. The purpose of this project is to design and develop a deepwater Electromagnetic sensor that can be used to detect these signals and filter out the unwanted noise at the same time. We use Electromagnetic (EM) waves because unlike other methods they can distinguish the potential hydrocarbon reservoirs due to their high resistivity value. This report shows in detail the design and development of a detector that implements the fluxgate technology. First we developed a single fluxgate and it was tested for sensitivity under a variety of frequencies. Then 5 more fluxgate units were fabricated and different configurations and orientations were tested. The final design which is a hexagon detector was fabricated based on the results obtained and sensitivity tests were performed on this design. The use of six fluxgates instead of only one improved the sensitivity by about 1000%. It was concluded that this new design was the best design as it is easy to implement, easy to manipulate and also cost effective. This design can be used for seabed logging as it proved to be sensitive at frequencies as low as 1 KHz.

ACKNOWLEDGEMENTS

First I would like to give an honor to God for His continuous everyday blessings.

Greatest gratitude goes to my supervisor Professor Dr Noorhana for her continuing dedication, motivation, patience and leadership on this project, and on this particular field of Electromagnetism in deep sea hydrocarbon exploration.

My gratitude also goes to my final year project colleagues for their great team work and support on this project. And I would like to thank my whole family and friend for their spiritual support and kindness.

And finally my sponsor (PETRONAS) and the great Universiti Teknologi Petronas for making me part of their family over the years I have been with them in this great country of Malaysia. I thank them for seeing a potential in me and investing in me by imparting knowledge and granting financial support.

TABLE OF CONTENTS

LIST OF TABLES

LIST OF FIGURES

CHAPTER 1
INTRODUCTION

1.1 Background of study

Seabed logging is a new and fast growing innovative tool, used to detect remote hydrocarbon reservoirs. This method uses the Electromagnetic imaging technology to strategically map the resistivity of the geological strata beneath the sea floor. SBL is a fast growing technique in oil and gas exploration because it achieves 90- 95% accuracy. While the commonly used method, which uses seismic waves, can only achieve 20 – 30 % accuracy. [1] There are different kinds of detector technologies and the most trusted are SQUID and Fluxgate, with the former being the most sensitive. However our project shall use the latter as it shall be thoroughly discussed in our report.

1.2 Problem statement

Designing and manufacturing detectors used for deepwater oil and gas exploration can be very challenging. Although detectors used for this purpose are very powerful however based on a study done by A.G Nekut and Brian R. Spies, on "Petroleum Exploration Using Controlled Source Electromagnetic methods"; it is still a challenge to acquire signals because of the decay in signal strength due to the long distance travelled($\geq$1500m) beneath the seafloor. Much cost in deep probing is incurred from advanced signal processing done to receive much clearer signal which can be useful for the process. A detector that can receive low frequency signals($\leq$1 KHz) and immediately filter and amplify is required.

1.3 Solution

- We have designed a new kind of an Electro Magnetic wave sensor using the fluxgate technology with the capability to detect EM signals as low as 1 kHz.

- This new invention consists of six fluxgates in a hexagon orientation. This arrangement enhances the effectiveness of the receiver as it maximizes reception from different angles.

- The implementation of six fluxgates in our new invention increases detection by over 1000% as compared to one fluxgate implementation.

- This new detector can receive and immediately amplify and filter the signal to eliminate the need for filtering during signal processing.

1.4 Objectives

- To utilize the PSpice tool in designing and simulating the optimum filter and amplifier suitable for our detector.
- To design a detector that can be used for seabed logging (at low frequencies as low as 1 kHz).
- To design a detector that can filter out the unwanted signals (noise) and amplify the signal before it can be sent for processing.
- To implement the fluxgate technology in the design.

1.5 Scope of study

This project involves detailed research on the design and mechanism of deepwater EM sensors. Also, software design tool skills and knowledge is required (PSpice software was used for our design). In addition, knowledge of the material characteristics suitable for Fluxgate design and fabrication is necessary.

CHAPTER 2
LITERATURE REVIEW

2.1 Seabed logging

Since Michael Faraday, in the early 1800's, discovered that a changing flux induces an electromotive force; Electromagnetic theory has been increasingly gaining attention. Today, almost all our technology is based on this ingenious discovery. [2]

In the year 2000 Statoil tested and succeeded the method for direct hydrocarbon detection in deep waters. Two years after that, the EMGS (Electro Magnetic GeoServices) was born and Seabed Logging was implemented. [3]

Since then EMGS has conducted more than 250 surveys, and the technique has been widely accepted by several of the world's leading oil and gas companies including PETRONAS, Chevron, Schlumberger, Shell, Statoil and BP.

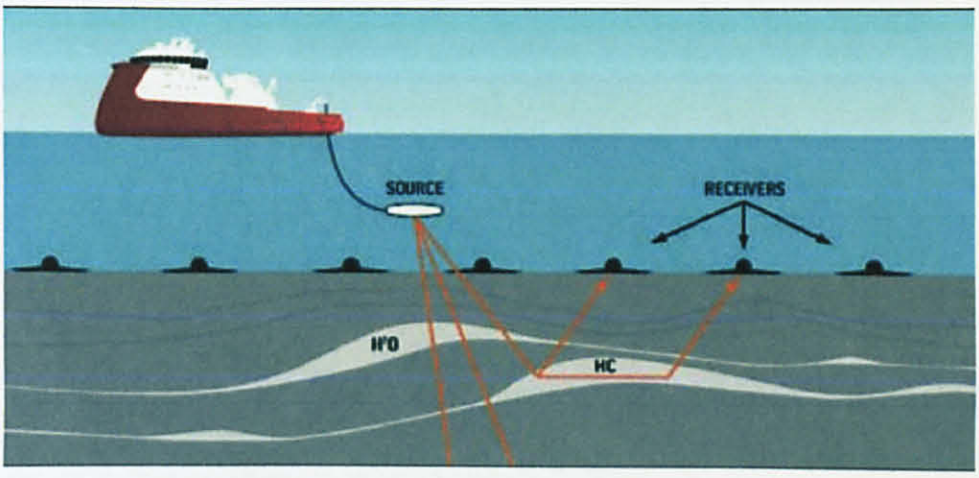

Figure 1 Seabed logging process

The basis for seabed logging is, the use a mobile EM signal source and an array of seafloor electric field receivers. The low frequency signal is reflected against the strata deep beneath the seafloor and it bounces back up at an angle into the sensor, where it is transmitted.

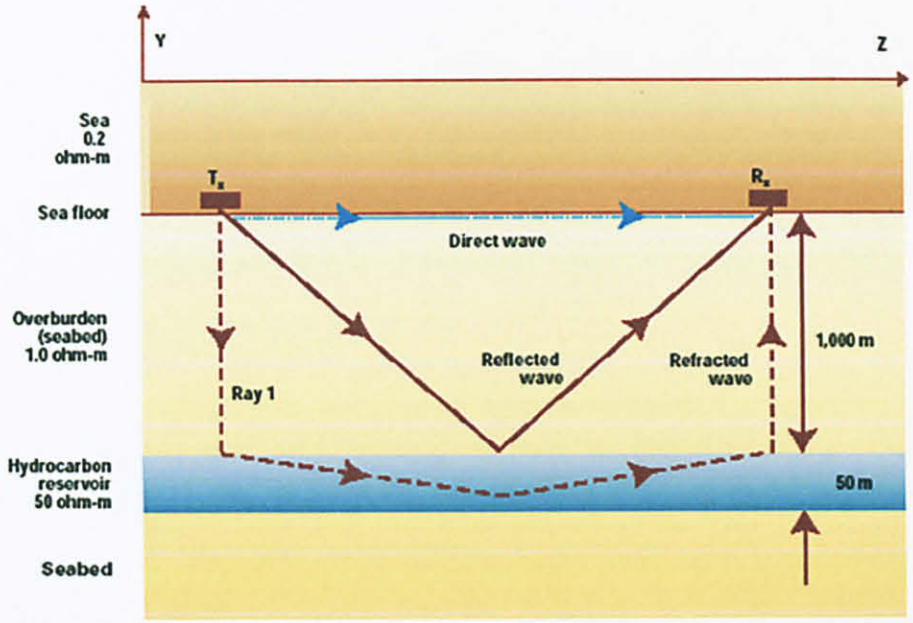

Figure 2 Wave propagation paths in a hydrocarbon reservoir

This new technology has great potential as far as the future of deep water oil and gas exploration is concerned. It is very fast since it uses real time imaging.

CSEM (controlled source electromagnetic) method is very reliable because it uses electromagnetic waves to acquire resistivity mapping for detection of hydrocarbons. The EM wave can penetrate into the rock as deep as 6000m. [4]- [10]

However the accuracy of this technology relies majorly on the sensor network on the sea floor, and their ability to detect the reflected EM waves. Hence on this project we are focusing on the design and implementation of an EM wave sensor for suitable for the seabed logging process.

2.2 EM wave detectors

There are different kinds of EM sensors but the most popular in the field of hydrocarbon detection are the fluxgate sensor and the squid sensor. The reason these two technologies are mostly applied in this field is because they are highly reliable and efficient in low-field-sensing applications. [8]

2.2.1 SQUID (Superconducting Quantum Interference Device)

This is the most sensitive low-field sensor in the industry. This technology was developed in 1962 based on the theory of Brian J. Josephson. As show in Appendix A, the SQUID magnetometer can detect extremely low fields from several femtoteslas, up to 9 teslas. [11]

However, the Squid has one major disadvantage. It requires constant cooling to liquid helium temperature (4 Kelvin). This was ruled not feasible for our design requirements since such cooling can be highly expensive, and also requires specialized knowledge and skill.

2.2.2 Induction coil detector

Induction coil is the one of the commonly used methods of magnetic sensors [12]. This is a fairly easy technique with a straight forward operating principle. Compared with other kinds of detectors it is also easy to manufacture in a very short time and using a limited supply of equipments. The only material required is the winding wire. There are two types of design methods used to implement this kind of detector (i.e. air filled coil or ferromagnetic core coils).

This sensor measures a voltage response proportional to the time rate of change of the magnetic field in the EM bandwidth. Comparison of measured voltage and magnetic-field data show that the two sets of profiles have quite different characteristics. The magnetic-field data is better for identifying, discriminating, and interpreting good conductors, while suppressing the less conductive targets.

2.2.3 *Fluxgate*

This is the 2nd most sensitive devise used for hydrocarbon exploration. This technology was developed in 1928 and it is most widely used because of its technical advantages. The fluxgate is highly sensitive as seen on appendix A, and it is also easy to apply as it does not require any cooling. It is simple and can be designed in the university lab. Therefore, in developing the sensor for our project we have chosen to use this technology. [13]

2.2.4 *Fluxgate design schematic and theory*

As we can see from figure bellow, the fluxgate detector consists of the ferromagnetic core and copper windings. This make up the primary element of the detector. The most important of these aspects is the core.

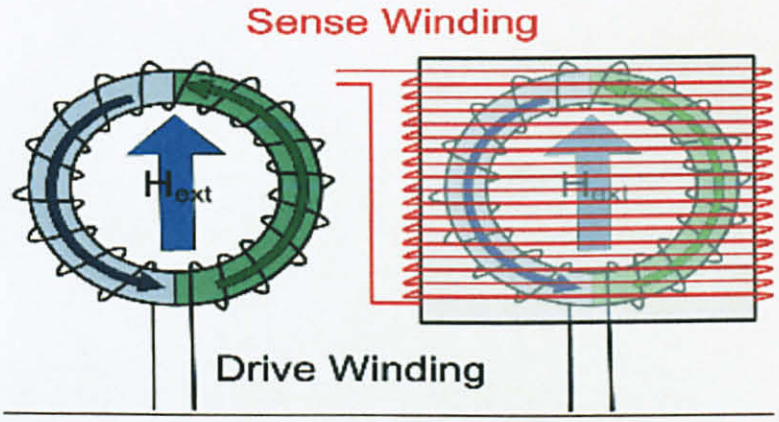

Figure 3 Fluxgate detector schematic

The windings around the core are called primary windings. Primary windings can also be called drive windings in this case, since they carry the drive current that brings about induction.

The **H** represents the external field which is very important in this concept as it brings about the 'sensing' in the coils. It is the external stimulus.

The windings that cover on top are secondary windings and we refer to them as sensor windings, since they will be detecting the disturbances caused by the incoming EM wave.

The core utilizes a concept called, magnetic saturation. This process referrers to the grouping of atoms in the core to form magnetic arrays. Ferromagnetic materials have a good dipole moment, which is why we going to use these materials to design the core of our fluxgate detector. A good dipole moment means they can be polarized by induction to a very high degree, and even after the removal of the external field, they remain partially magnetized. [13]- [22]

2.3 EM wave detection theory

As we can see from the figure, the EM wave travels as a 3 dimensional vector. It consists of the electric signal and the magnetic signal. This means that our fluxgate will be detecting only one axis of this signal, the magnetic vector axis. It is this component of the EM wave we are mostly concerned about in our sensor. This magnetic field will disturb the secondary induced **B** field as we explained above. It is this disturbance we shall base our findings. [2]

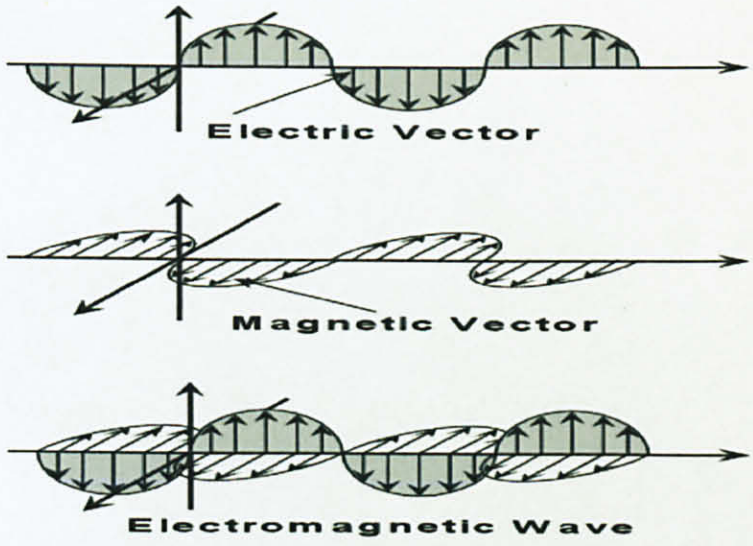

Figure 4 Electromagnetic wave components

2.4 Faraday law and Lenz's law

This design uses two fundamental electromagnetic laws, the Faraday's law and Lenz's law. Faraday law states that, a changing magnetic flux in a coil (primary coil) will induce voltage on the secondary coil.

Induced emf = - N dØ/dt [Faraday's law]

The key to this, is that the flux must be changing continuously for induction to occur. Refer to the figure below. Lenz's law states that, an induced electromotive force generates a circuit that induces a counter magnetic field that opposes the magnetic field generating the current.

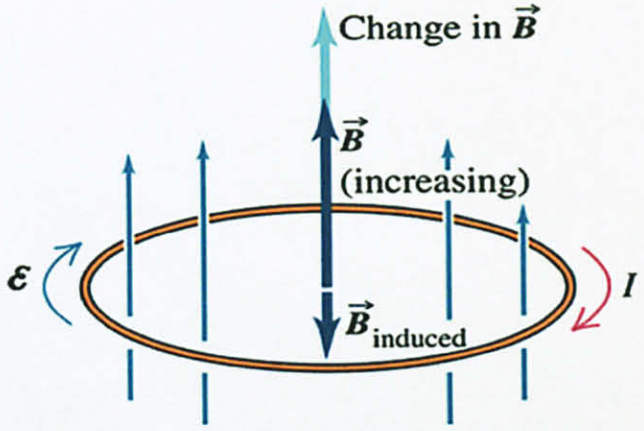

Figure 5 Faraday law and Lenz law illustration

This means that the **B** field induces current I in the clockwise direction. The current **I** in turn induce a B field in the onward direction, which opposes the original field that was initially going up. It is this opposition that we are concerned about in our fluxgate sensor. When the external EM signal comes into contact with the induced **B** field, it will cause a disturbance which will make a difference in the voltage being measured. This disturbance will be carrying the hydrocarbon information we require. [10]- [11]

CHAPTER 3
METHODOLOGY

3.1 Procedure identification

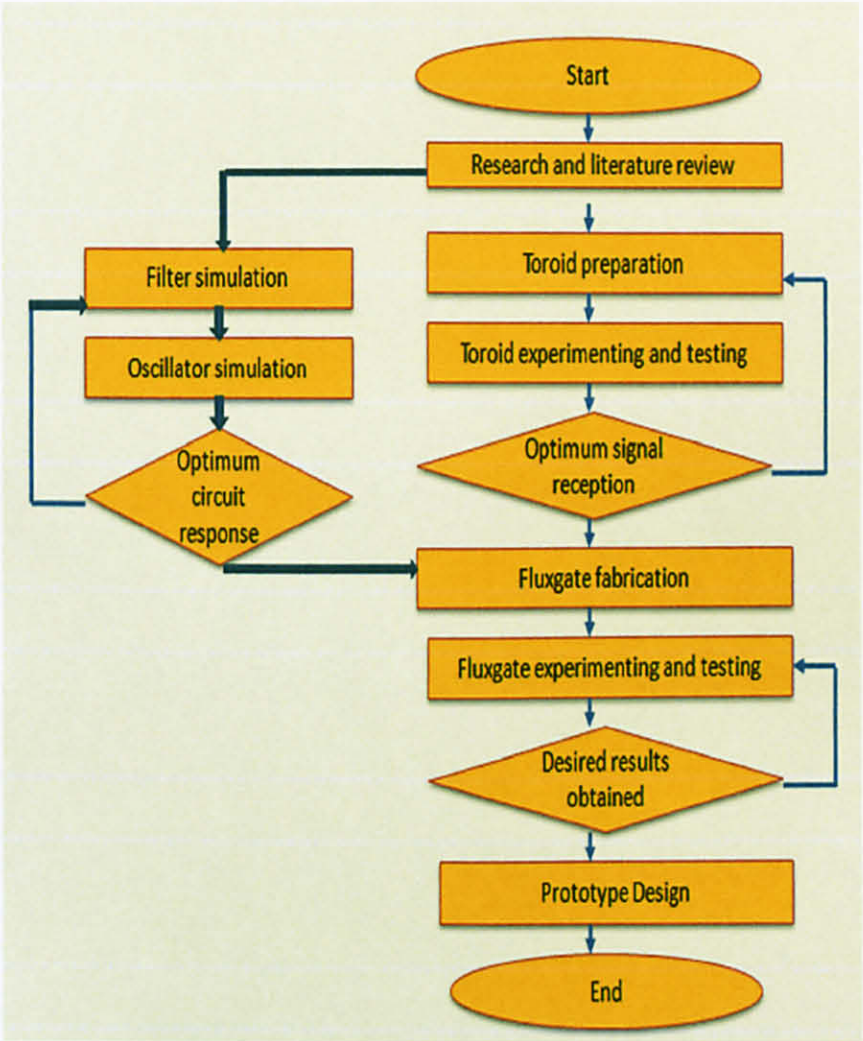

Figure 6 Project flow chart

3.2 Tools and equipment required

3.2.1 Tools

Table 1 List of hardware and software used to construct a fluxgate

HARDWARE	*SOFTWARE:*
• Copper wires with enamel lamination • Ferromagnetic core • Function generator • Power supply • Oscilloscope • Data logger; PC • Transmitter • Anacom2 board	• Pico Logger Recorder • PSpice

- AC waveform generator
  - Goodwill INSTEK GFG-8250A
  - 20 Volt peak to peak
  - Operating frequency of 1 to 5 MHz

- Oscilloscope
  - Tektronix TDS 3012B
  - 100 MHz

3.2.2 Filter and oscillator circuit simulations

Objective: The aim for this simulation is to determine the filter and oscillator circuit most suitable for our fluxgate sensor design. PSpice tool is used for all simulations.

Active filter:

A device that separates, passes, or suppresses electronic signals from a mixture of signals. Most filters separate signals according to the signal frequency content. Frequency selective filters are divided into passive and active filters. On this report we have designed different kinds of active filters in order to observe their different responses when certain variables are changed.

Table 2 Butterworth Band Pass Filter Simulation

Variables	C3 = [0.01uF TO 0.05uF] [Increment = 0.01uF]
Circuit	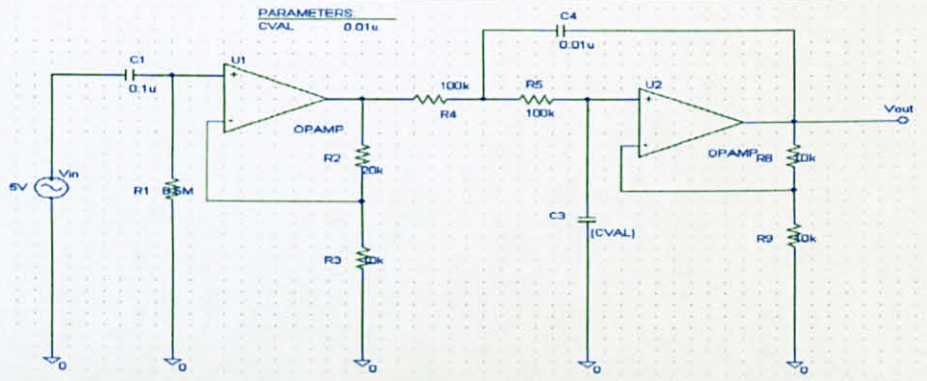
Simulation Output	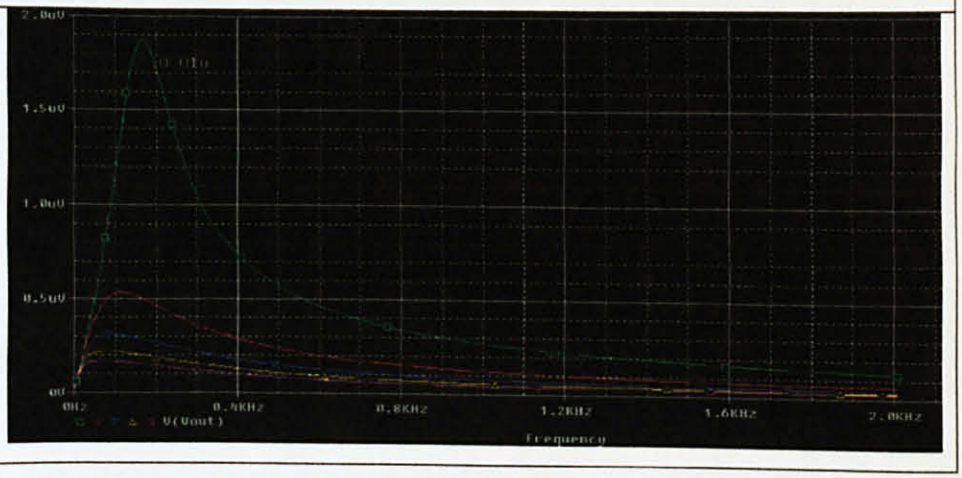

Table 3 Low Pass Filter Simulation

Variables	Circuit	Simulation Output
C2 = [0.01uF to 0.05uF] Increment [0.01uF]	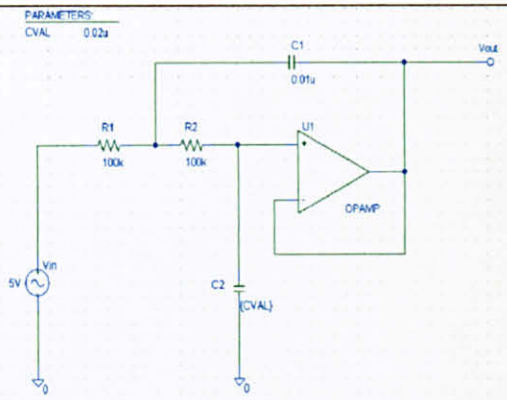	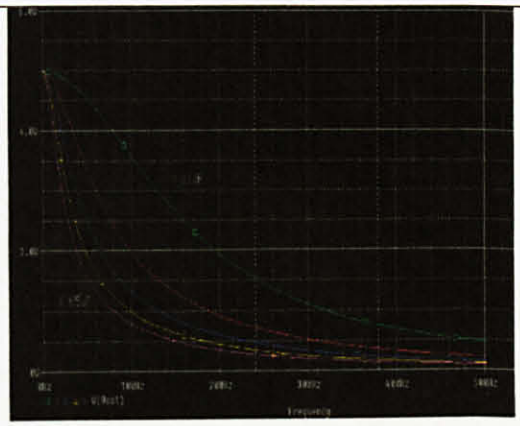
C1= [0.01uF to 0.05uF] Increment [0.01uF]	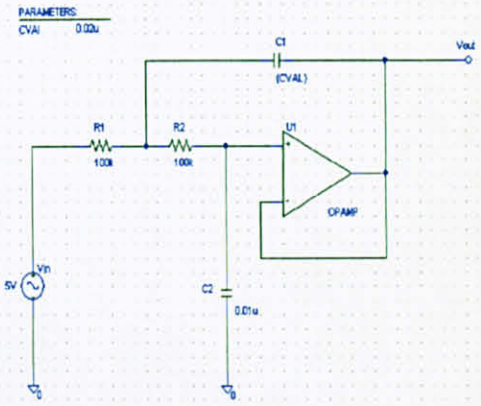	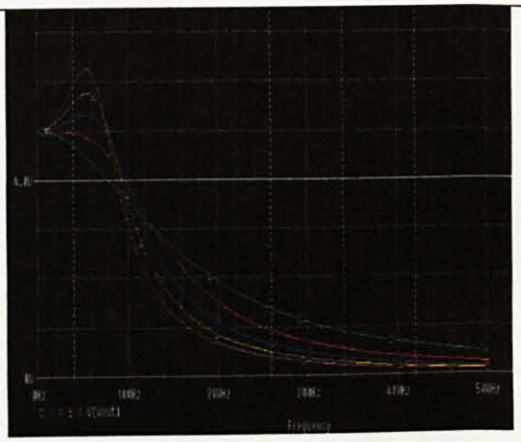
Negative feed back effect	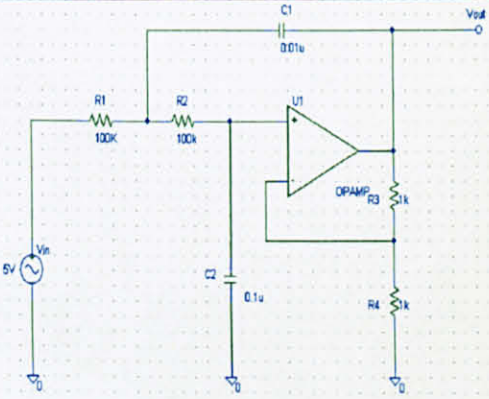	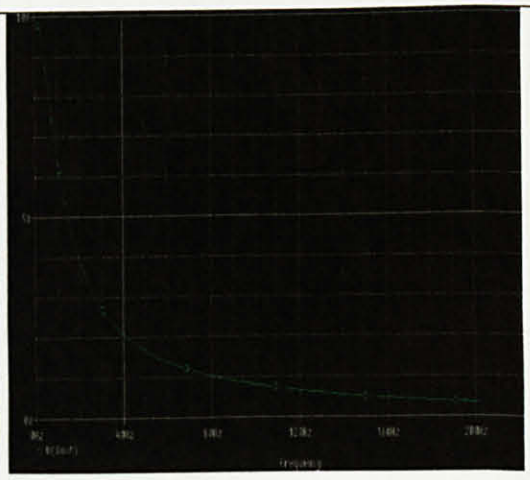

Table 4 High Pass Filter Simulation

Variables	Circuit	Simulation Output
R2 = [10kΩ to 20 kΩ] Increment [2kΩ]	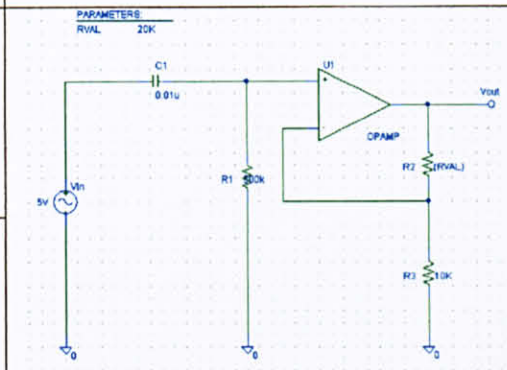	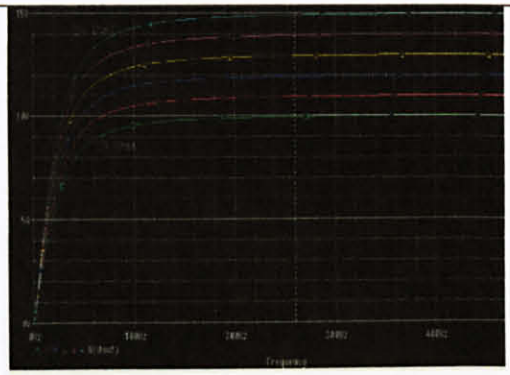
R3 = [10kΩ to 20kΩ] Increment [2 kΩ]	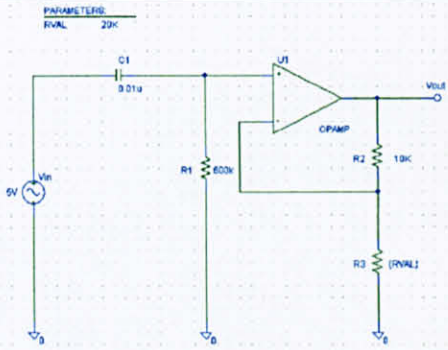	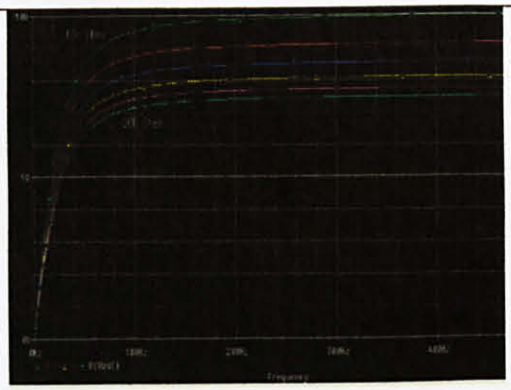
R1 = [100 kΩ to 500 kΩ] Increment [100 kΩ]	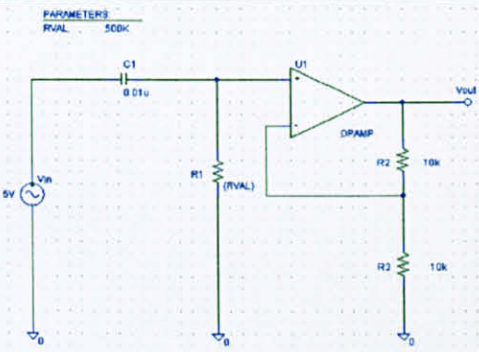	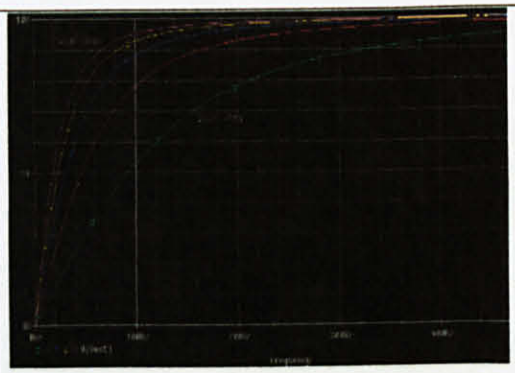
C1 = [0.01uF to 0.1uF] Increment [0.01uF]	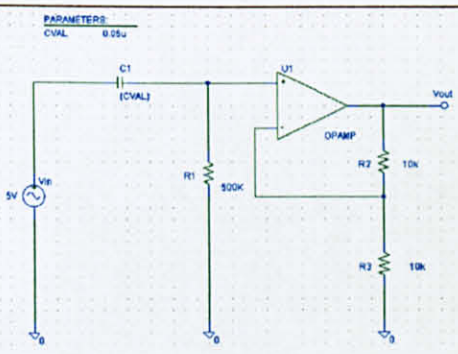	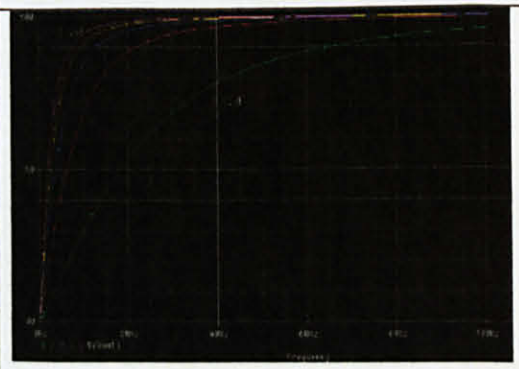

Table 5 State variable Band Pass Filter Simulation

Circuit	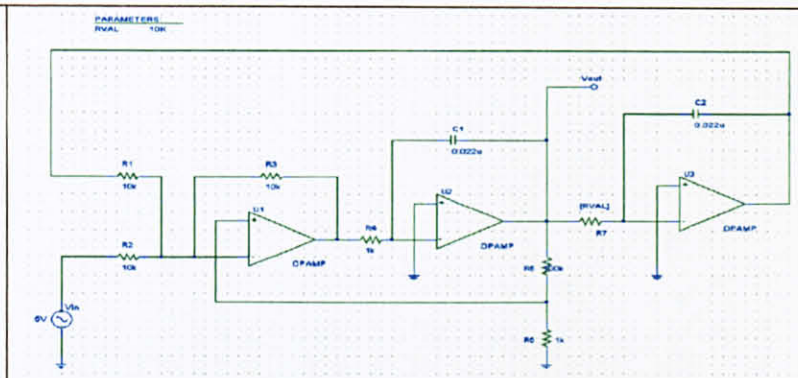	**VARIABLES** R7 = [2kΩ to 14 kΩ] [Increment] [2 kΩ]
Simulation Output	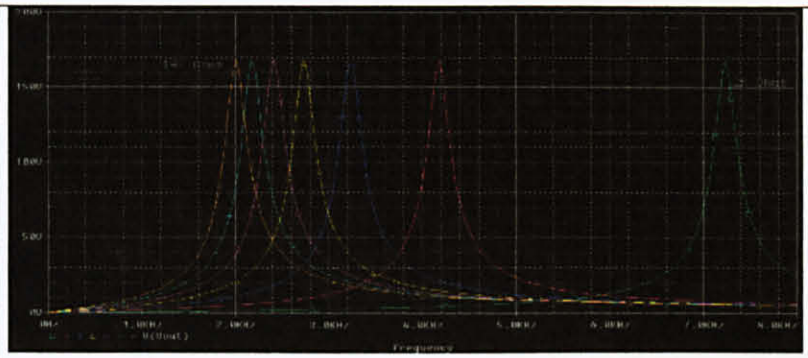	
Circuit	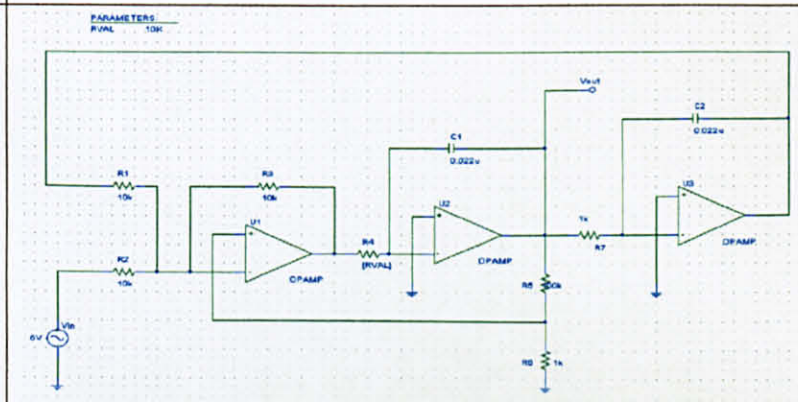	R4 = [2 kΩ to 14 kΩ] [Increment] [2kΩ]
Simulation Output	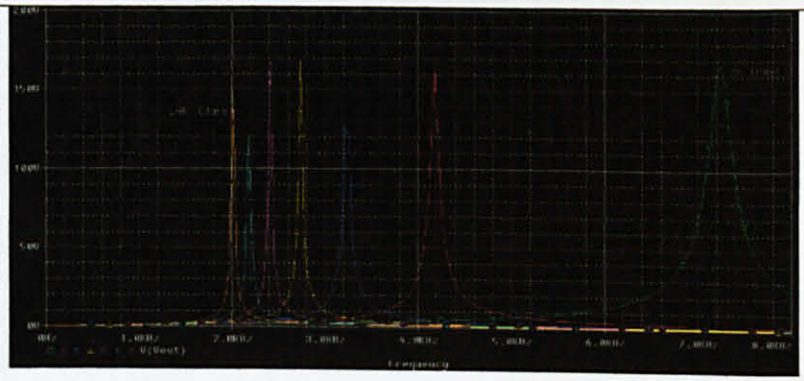	

Table 6 Multiple Feed Back Band Pass Filter

Variables	Circuit	Simulation Output
R1 = [20kΩ to 100 kΩ] Increment [20 kΩ]	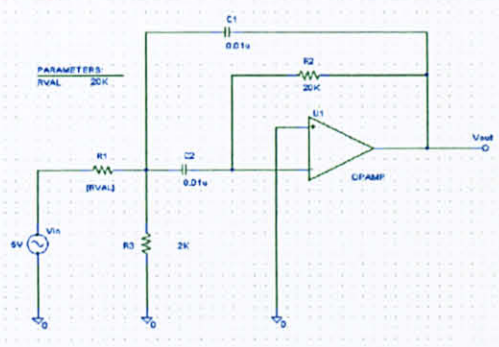	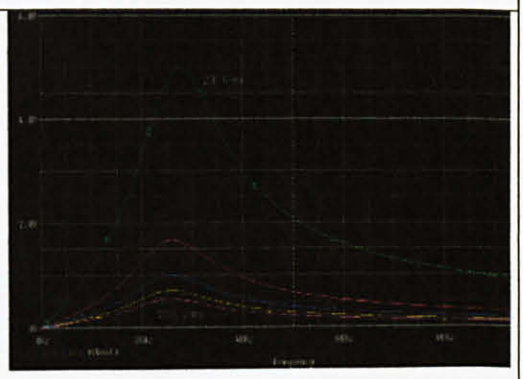
R3 = [20kΩ to 100kΩ] Increment [20 kΩ]	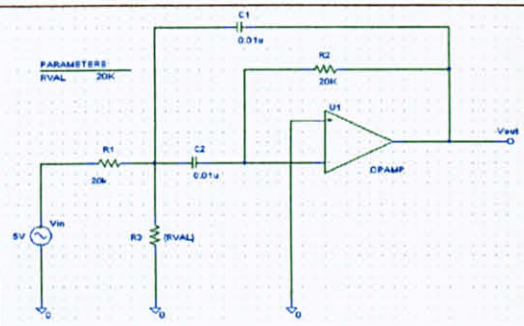	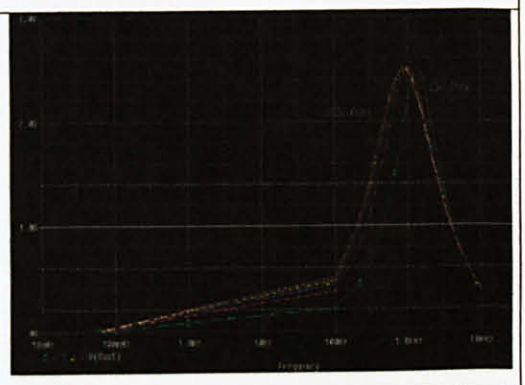
R2 = [20kΩ to 100 kΩ] Increment [20 kΩ]	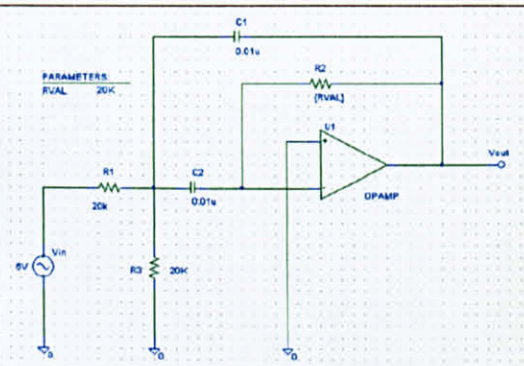	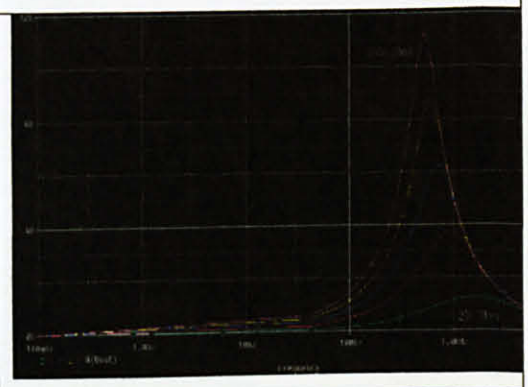
C1= [0.01uF to 0.1uF] Increment [0.01uF]	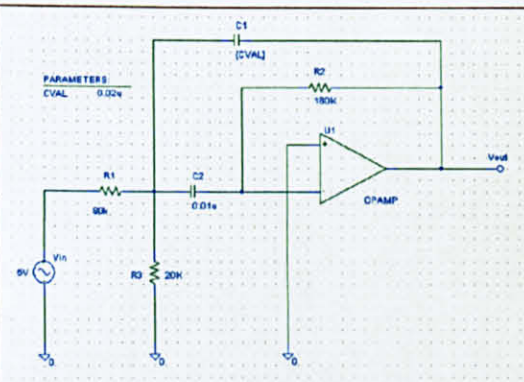	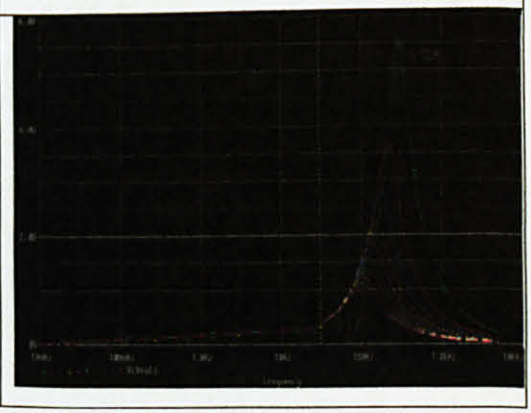

Table 7 Oscillator Circuit Simulation

Variables	Circuit	Simulation Output
R2= 2 kΩ	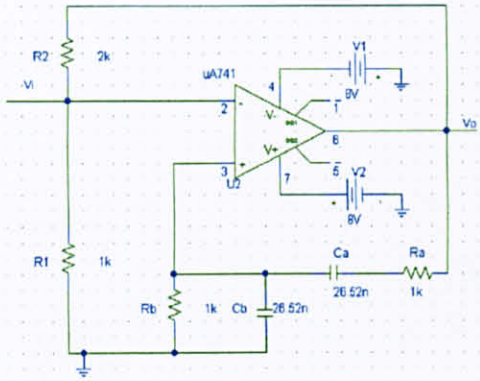	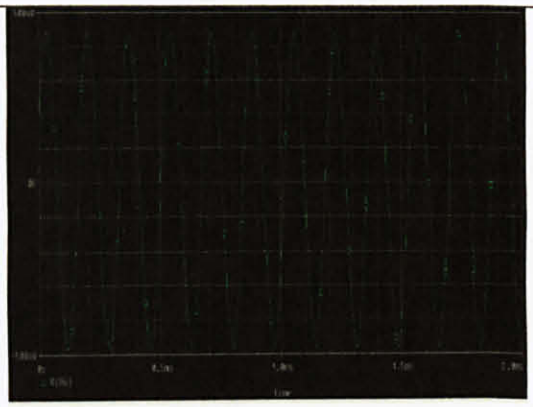
R2= 3 kΩ	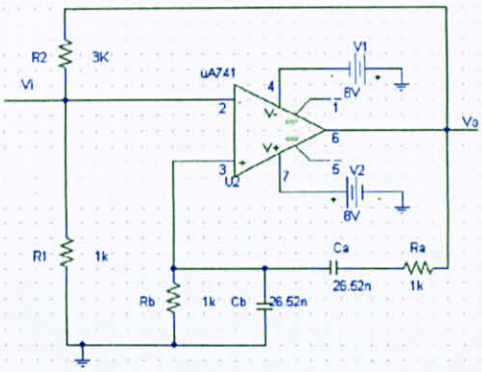	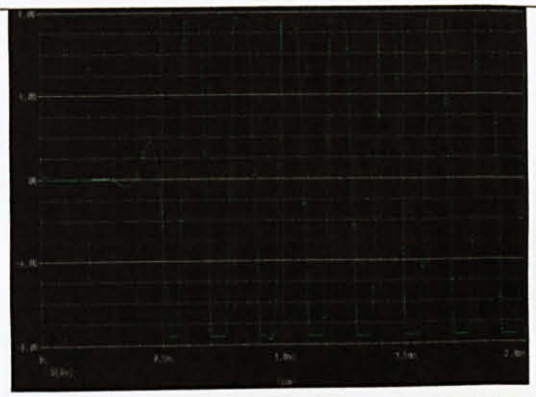
R2= 4 kΩ	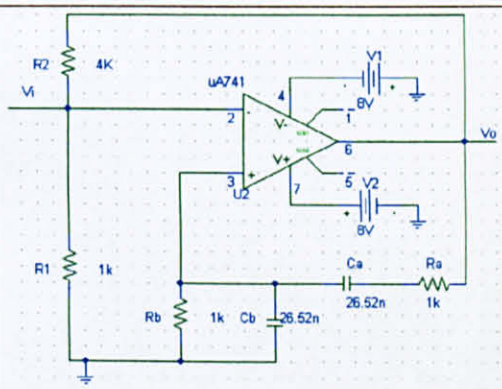	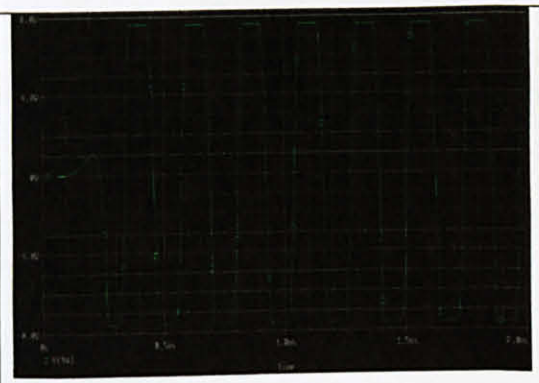
R2= 10kΩ	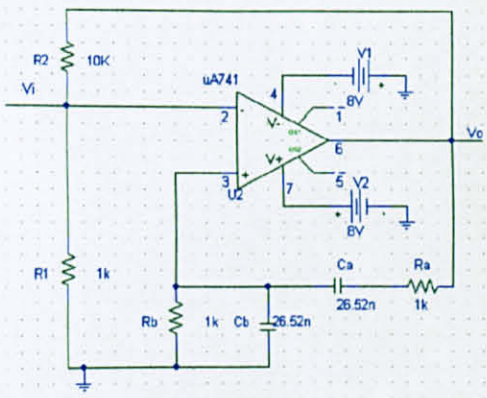	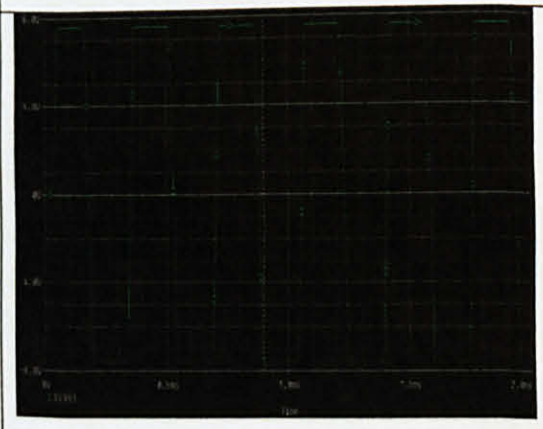

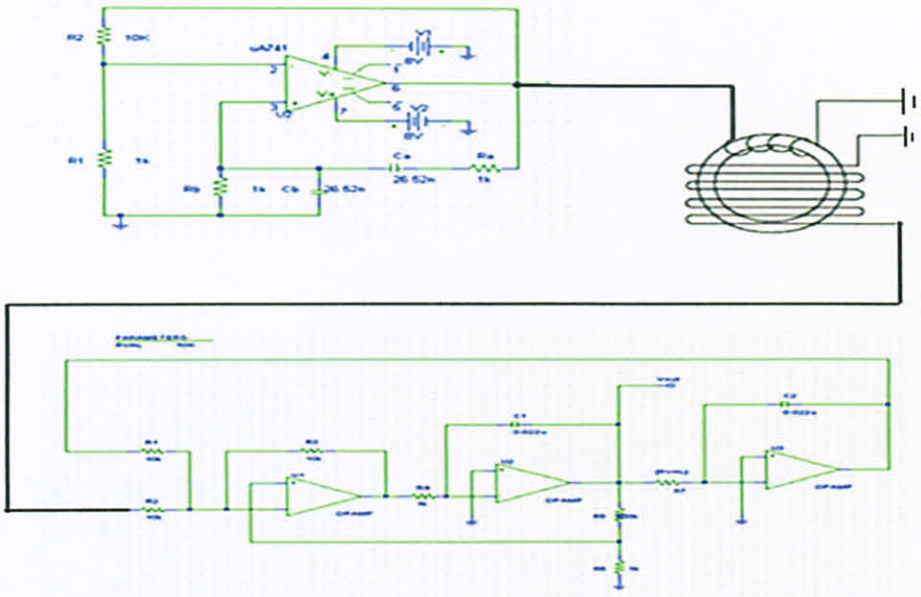

Figure 7 Design circuit with filter and oscillator implemented

Table 8 The design circuit analysis

$Q = (1/3)[R_5/R_6 + 1]$	$F_C = 1/ (2\Pi * R_7 * C_2)$	$BW = (f_O/Q)$
$R_5 = 100k\Omega$ $R_6 = 1k\Omega$ $Q = 33.7$	$R_7 = 7.23k\Omega$ $C_2 = 0.022\mu F$ $F_C = 1kHz$	$F_O = 1kHz$ $Q = 33.7$ $BW = 30Hz$
$R_5 = 100k\Omega$ $R_6 = 1k\Omega$ $Q = 33.7$	$R_7 = 1k\Omega$ $C_2 = 0.022\mu F$ $F_C = 7.23kHz$	$F_O = 17.23kHz$ $Q = 33.7$ $BW = 215Hz$

From the circuit analysis on the table above we see that the quality factor of the circuit based on the filter performance is 33.7. This is highly acceptable since it is above 10 and the band width is 30 Hz. However when R7 is varied to about 7 kilo ohms as shown, the band width increases to 215HKz. For our design we prefer R7 at 1 kilo ohm although the band width is narrow.

3.3 Toroidal equation derivation

$\oint_C \boldsymbol{H}.\, \boldsymbol{dl} = \boldsymbol{NI}$ [Ampere's law]

- Ampere's law states that the line integral of **H** around a closed path is equal to the current traversing the surface bounded by that path.[2]
- Also that, if the direction of **I** is aligned with the direction of the thumb of the right hand, then the direction of the contour **C** should be chosen to be along the direction of the other 4 fingers.
- According to the right hand rule associated with Ampere's law, the current is positive if it crosses the surface of the contour in the direction of the four fingers of the right hand, when the thumb is pointing along the direction of the contour **C.**

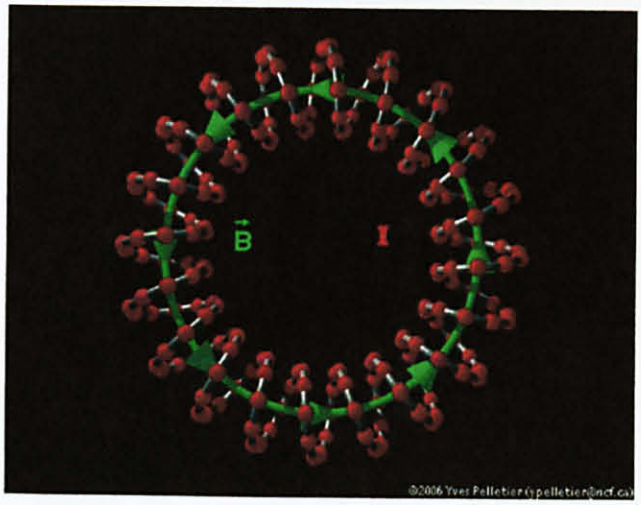

$$\oint_C \boldsymbol{H}.\, \boldsymbol{dl} = \int_0^{2\pi} (\hat{\phi}\, H).\hat{\phi} r\, d\phi$$

$$= 2\pi r H$$

Therefore, $H = NI / (2\pi r)$

3.4 Experiment #1: Determining the optimum turn ration using the data logger

Objective: The aim for this experiment was to determine the optimum turn ration of the drive winding to the sensor winding.

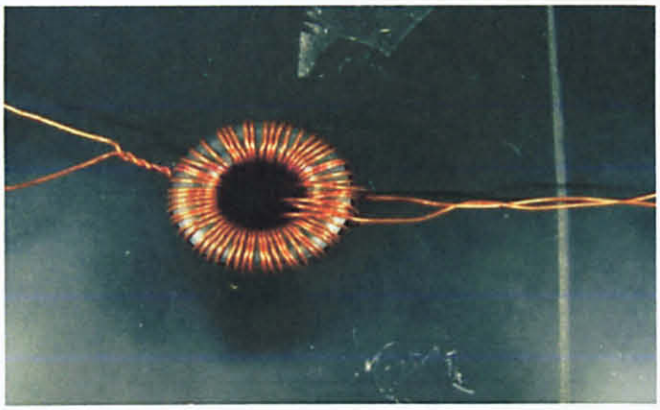

Figure 8 Toroidal core fluxgate

A 20 turn (primary coil) toroid was prepared as shown on the figure above

The secondary windings (sensor windings) were fixed at 5 turns for the entire experiment.

The drive wings (primary windings) were varied from 10 to 60 wings with increments of 5.

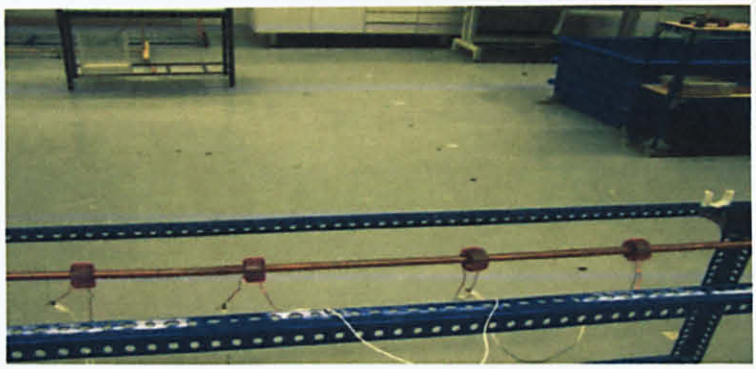

Figure 9 Monopole transmitter and a function generator

A monopole transmitter was connected as seen on the figure above with 4 magnetic feeders.

The monopole transmitter was turned on to transmit at 1 kHz.

A square wave was used for the experiment.

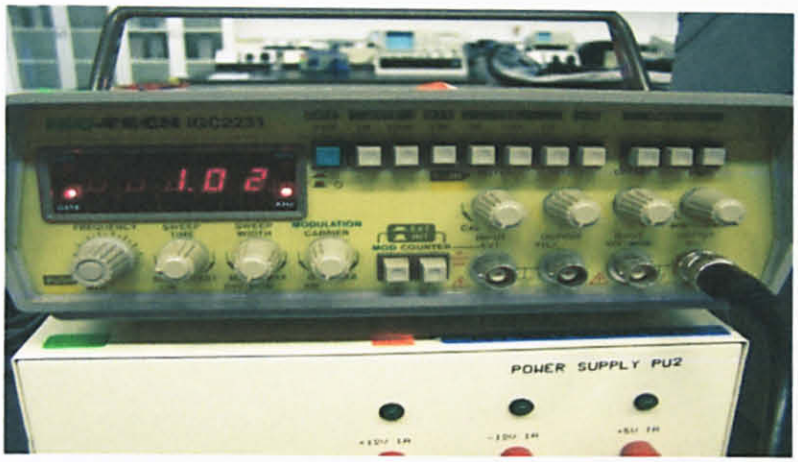

Figure 10 Function generator feeding the 1 KHz wave to the transmitter

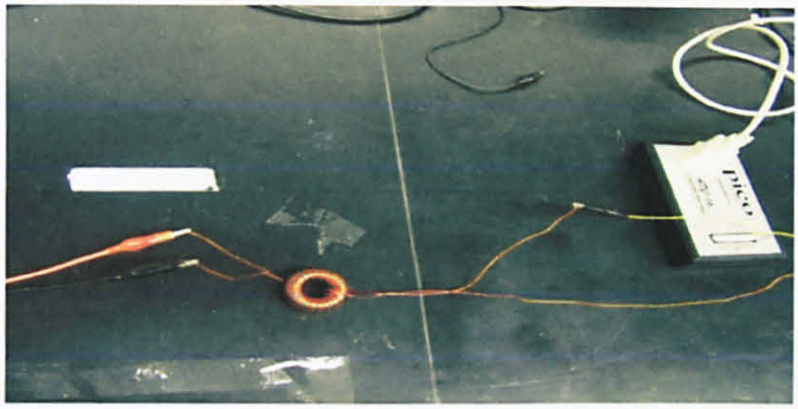

Figure 11 Toroidal core fluxgate connected to the data logger

The sensor coils were connected to the data logger which was in turn connected to the pc.

The drive turns (primary turns) were connected to a function generator to produce a change in flux.

The signals were then recorded using 1 minute intervals of 100 samples per minute.

The results for this experiment are illustrated and discussed in chapter 4, section 4.1.1.

3.5 Experiment #2: Determining the optimum sensor orientation using the Anacom board

Objective: the aim for this experiment was to determine the the best fluxgate positioning, for optimum sensing capability.

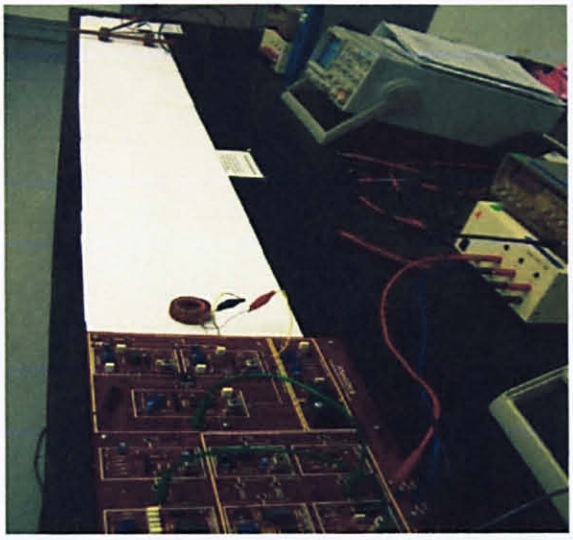

The toroid was placed flat on the table as seen on the picture in the left. The hollow side of the toroid was facing up. The toroid is connected to the Anacom board which has a built in signal amplifier and filter. The transmitter is at the 1.5m distance and transmitting at 1 MHz's

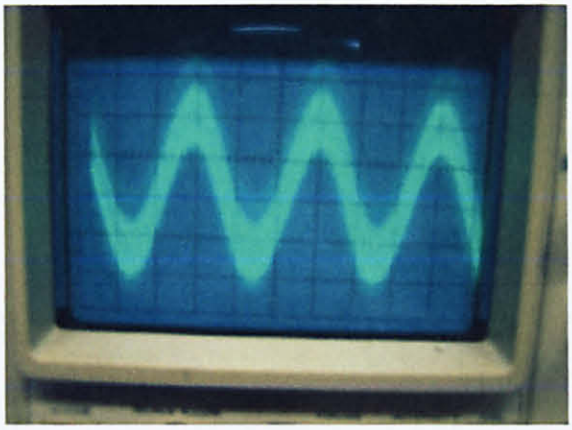

The response has a lot of distortion and the wave received is unclear because of the noise. This shows that this position is not desirable for our detector design.

Figure 12 Fluxgate horizontal orientation setup

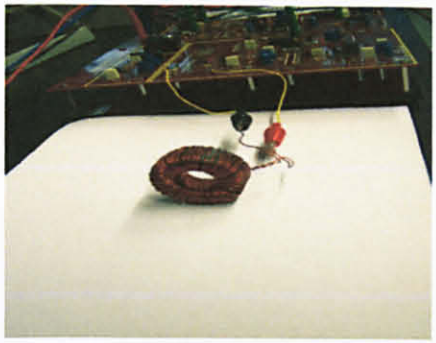

The toriod was positioned in a vertical direction, with the inner hole facing the direction of the transmitter and the incoming signal.

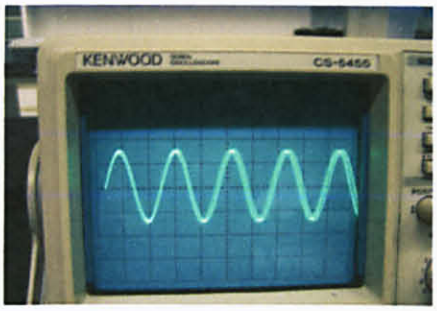

The response to this orientation showed a clear signal with the same amplitude as the input signal. This indicates that with this positioning method the noise is very low, hence the clear signal in observed.

Figure 13 Fluxgate vertical orientation setup and response

3.6 Experiment #3: Fabricating and testing a complete single Fluxgate unit

Objective: The aim for this experiment was to produce a fluxgate and testing it for optimum results.

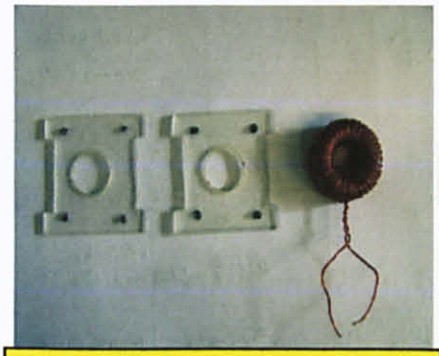

The toroid seen above was manufactured using the ratio 3:7 for the windings.

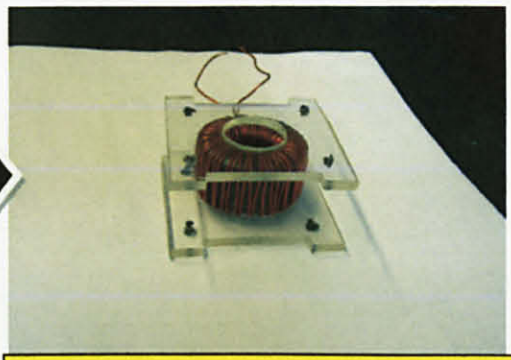

The Perspex material was used as means to hold the outer windings since it does not interfere with the signal

The complete single fluxgate was produced and tested in order to determine the optimum result (clear response).

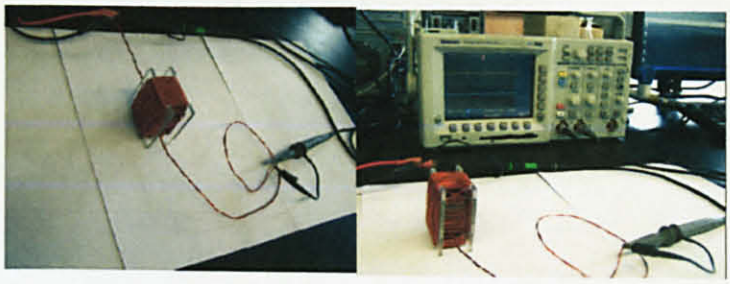

3.7 Experiment #4: Optimum angle positioning

Objective: The aim for this experiment was to determine the most effective orientation and shape for our detector design.

3.7.1 The side-by-side fluxgate orientation

The 1st part of experiment 4 was to position two fluxgates side-by-side to each other.

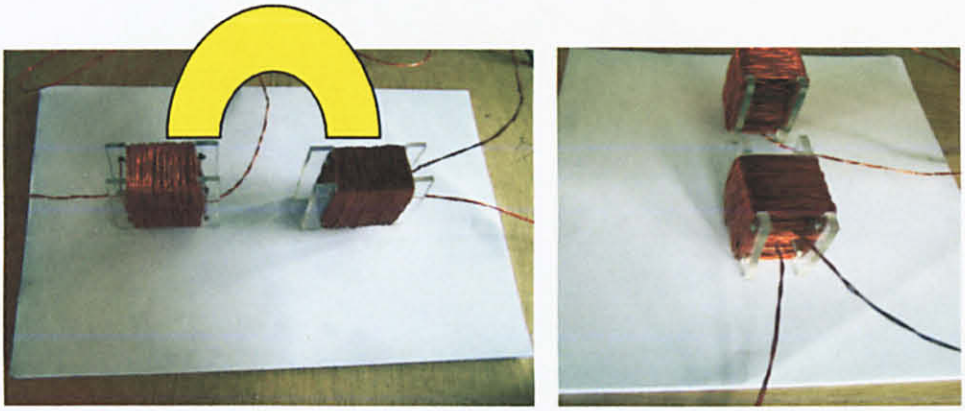

Figure 14 On the above illustration we can see a 180 degree separation (side-by-side positioning).

3.7.2 The decreased angle of orientation fluxgate setup

The 2nd part of experiment 4 was to vary the positioning of the two fluxgates to determine the effect of the decreased angle of separation between the fluxgates.

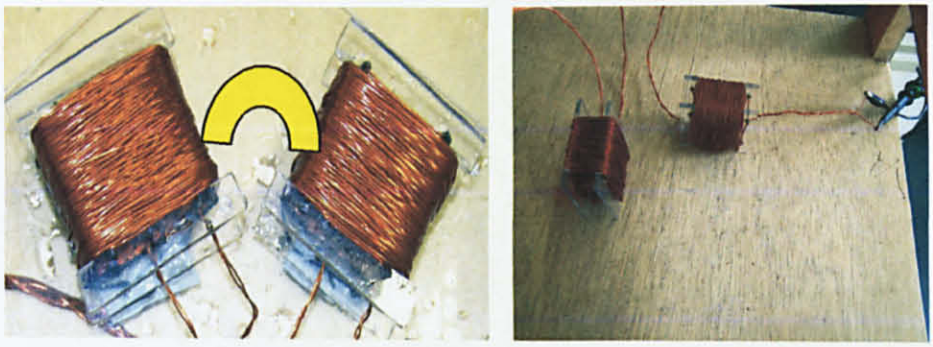

On the illustration above we observe a decreased separation angle between the fluxgates

The results for these configurations are shown and discussed on chapter 4.

3.8 Experiment #5: Prototype fabrication and testing

Objective : The aim for this experiment was to manufacture the final design (hexagon shaped fluxgate detector) and test it in salt water to determine its sensing capabilty.

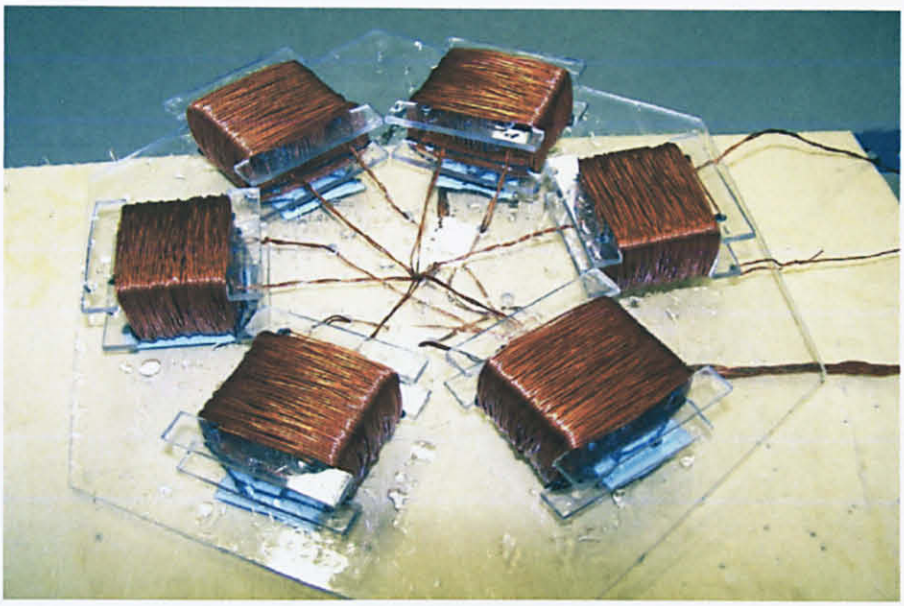

Figure 15 Final prototype (hexagon shaped)

On the final design as we see from figure 15, six fluxgates were used in a hexagon shape arrangement. This new detector was then tested in salt water as seen on figure 16 bellow. The results and discussion on this test are illustrated on chapter 4.

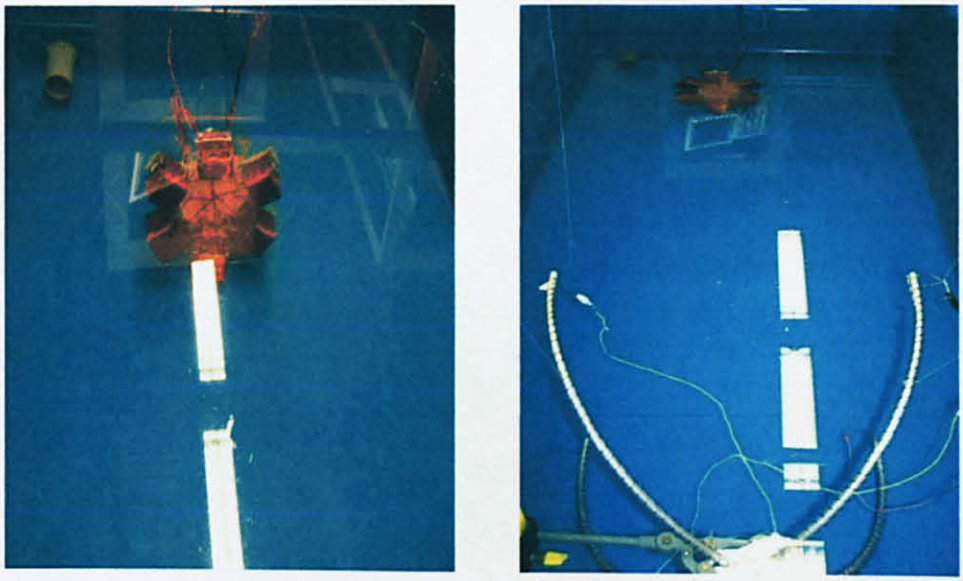

Figure 16 Underwater test of the detector conducted at the lab in a tank filled with salt water of 1.18 Ωm conductivity. The detector and transmitter are placed 1.9 m apart and completely immersed in the salt water.

CHAPTER 4
RESULTS AND DISCUSSION

4.1 Results

4.1.1 Experiment #1 results: optimum turn ratio determination

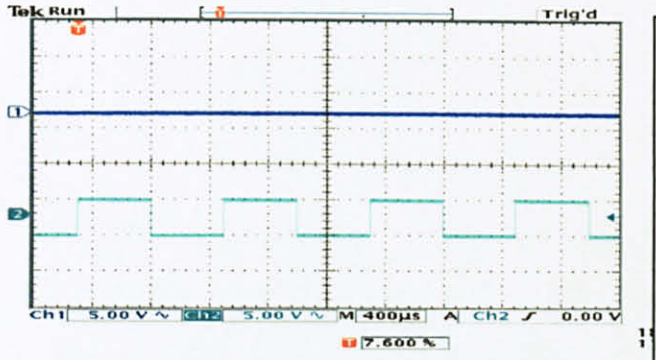

Figure 17 Input signal to the drive windings

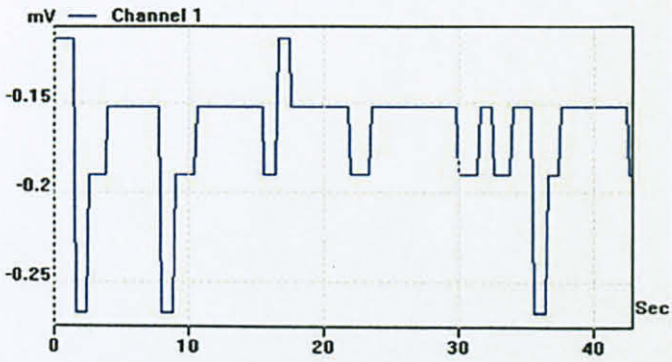

Figure 18 Voltage response without transmission

DISCUSSION

Figure 16 on the left is an input signal which serves as excitation for the drive windings. No transmission signal was sent at this point since the transmitter was off. Only the sensor was turned on. Figure 17 is the output response. It is clear that the graph takes the form of the input signal. It would be almost a perfect square wave if it was not for the distortions as we can see. These disturbances can be related to the frequencies in the surrounding environment. Which is the reason why our sensor will need shielding, as to divert these unwanted signals.

Table 9 Sensor response with changing number of drive windings after the transmitter was turned on

Number of turns	Voltage response vs. time	Discussion
20	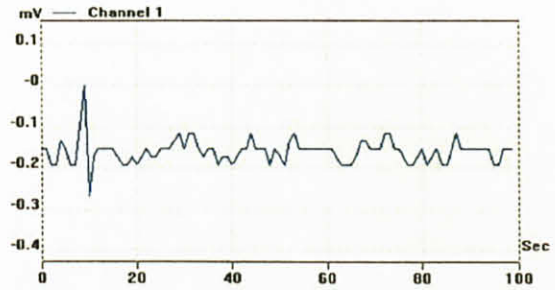	Poor signal clarity with a lot of distortions. Signal is not visible
30	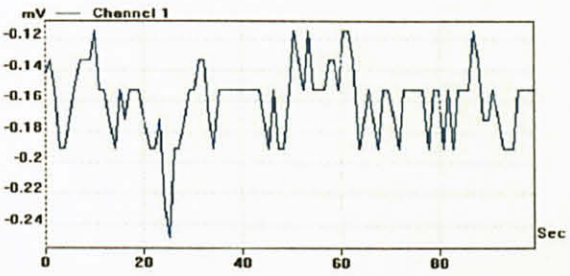	Better signal clarity with distortions still present.
40	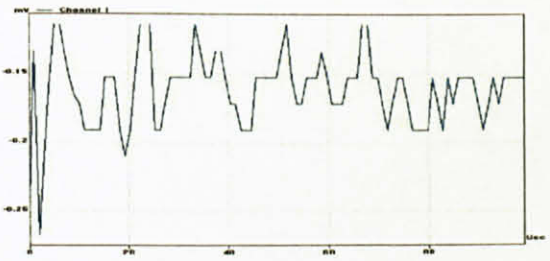	Improved signal clarity. Distortions still visible however.
50	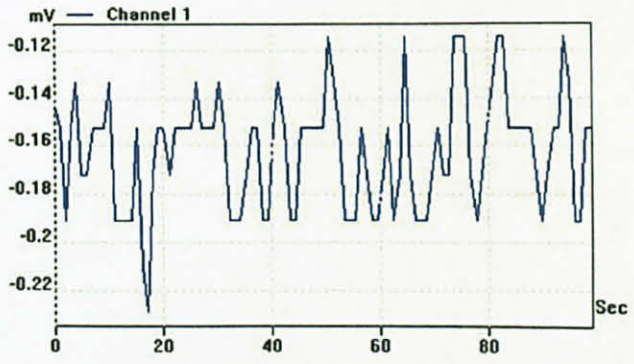	Much improved signal. At this point not much change was experienced when the number of turns was increased.

4.1.2 Experiment #3 results: Single fluxgate test

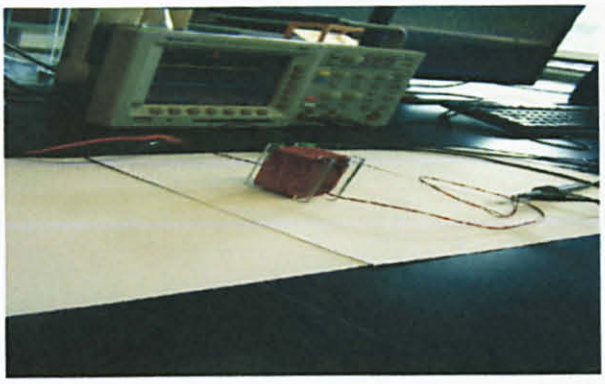

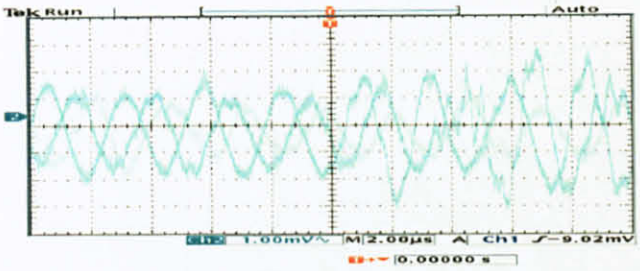

Figure 19 Response at 300 KHz

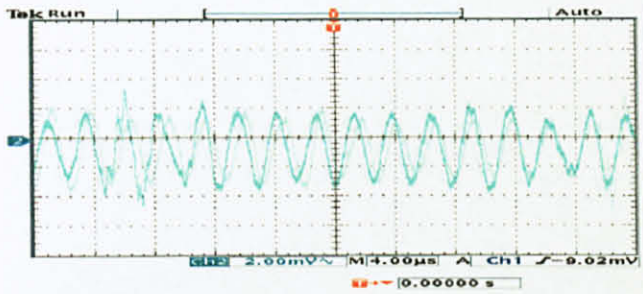

Figure 20 Response at 340 KHz

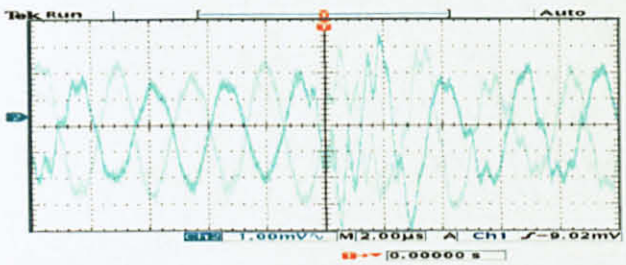

Figure 21 Response at 400 KHz

DISCUSSION:

The fluxgate experiment was conducted using a single fluxgate sensor as seen on the picture illustration on the left.

The maximum distance between the fluxgate and the transmitter was 2.5m. This maximum distance was chosen because it was observed that at distances exceeding 2.5m the fluxgate experienced more noise from the surroundings.

As seen from the results of figure 18 up to figure 24, the signal clarity starts to be sharp at around 440 KHz to 460 KHz. However the detector starts to detect at about 300 KHz.

At this point we have established that a single fluxgate detector is not enough to lower the detector sensitivity down to 1 KHz as desired. It can only go as low as 300 KHz.

The rest of the results are illustrated on the next page.

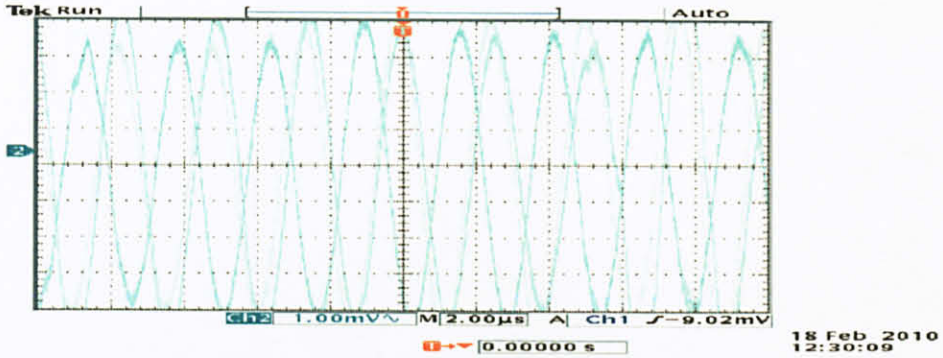

Figure 22 Response at 420 KHz

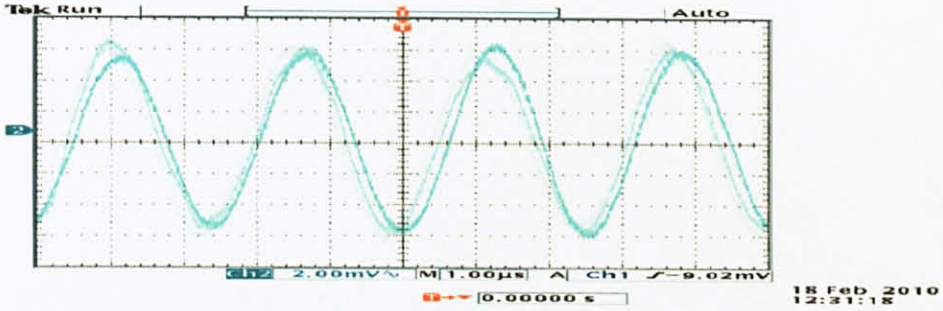

Figure 23 Response at 440 KHz

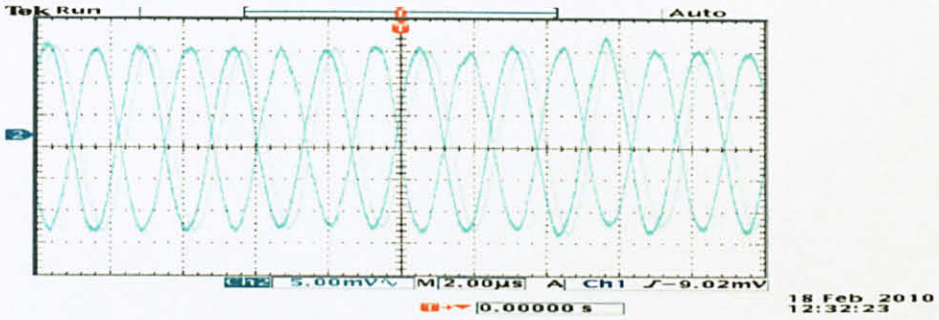

Figure 24 Response at 450 KHz

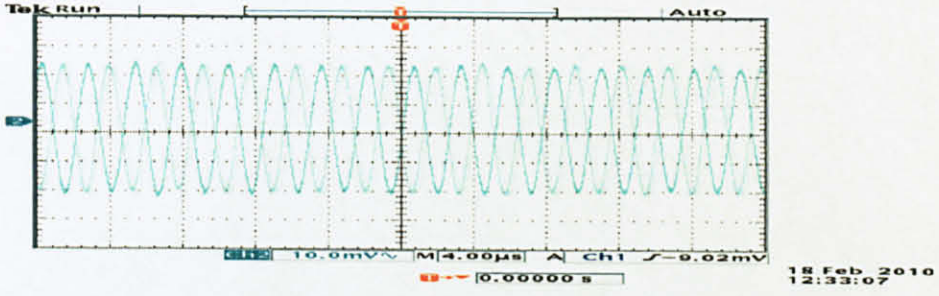

Figure 25 Response at 460 KHz

4.1.3 Experiment #4 part 1results: Side-by-side fluxgate orientation setup.

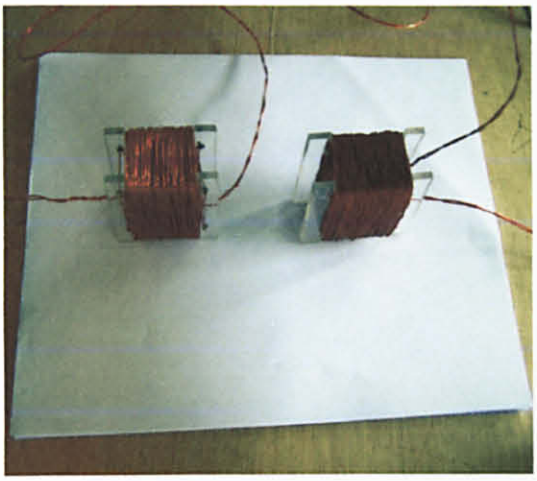

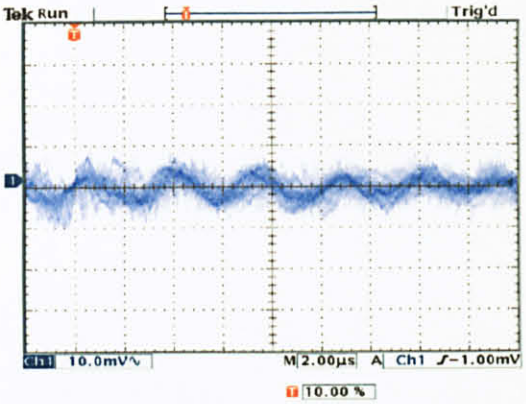

Figure 26 response at 280kHZ

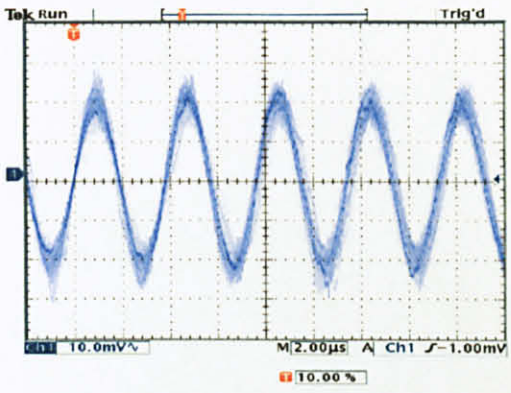

Figure 27 response at 300kHZ

DISCUSSION

Different position configurations were used in order to establish an ultimate model.

From these position configuration it was observed that, placing two fluxgates, side by side, connected in series does in deed result in a more improved wave form. As it can be seen on the picture illustration on the left, two fluxgates are placed side-by-side.

The fluxgates which were used both had 145 secondary turns and 62 primary turns. Their fabrication was based on the 3:7 ratios.

From figure 25 to figure 30, it is evident that the sensor (consisting of two fluxgate units) starts to detect a signal as low as 280 KHz. And signal clarity starts at about 300 KHz to 400 KHz.

This is an improvement from the single fluxgate design.

The rest of the results are illustrated on the next page.

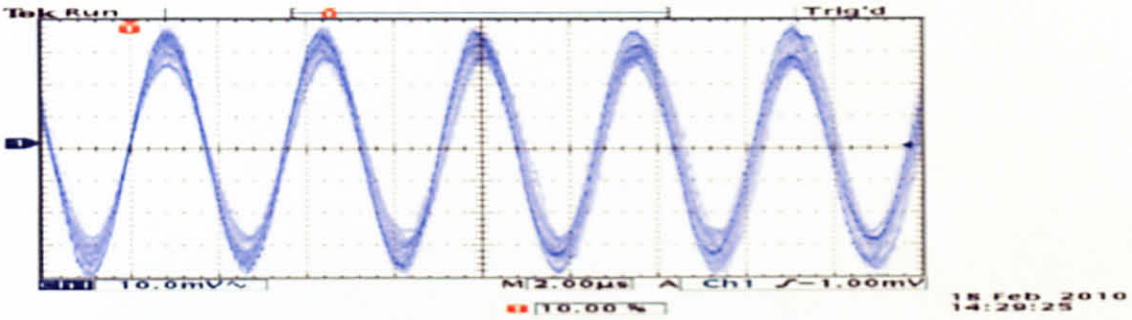

Figure 28 response at 350kHZ

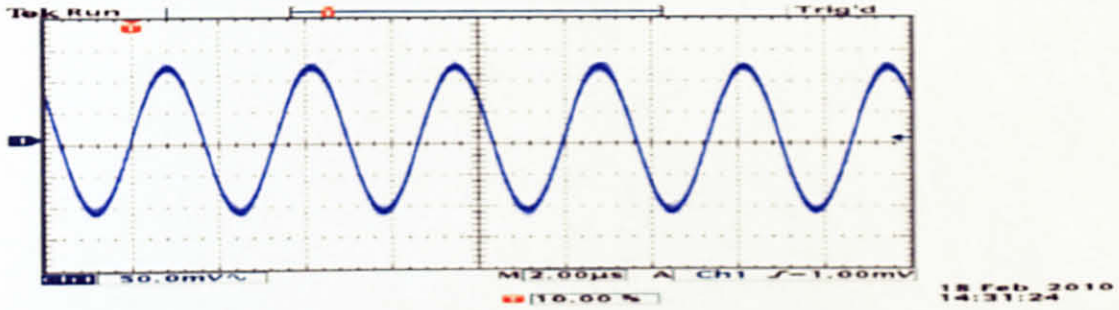

Figure 29 response at 370kHZ

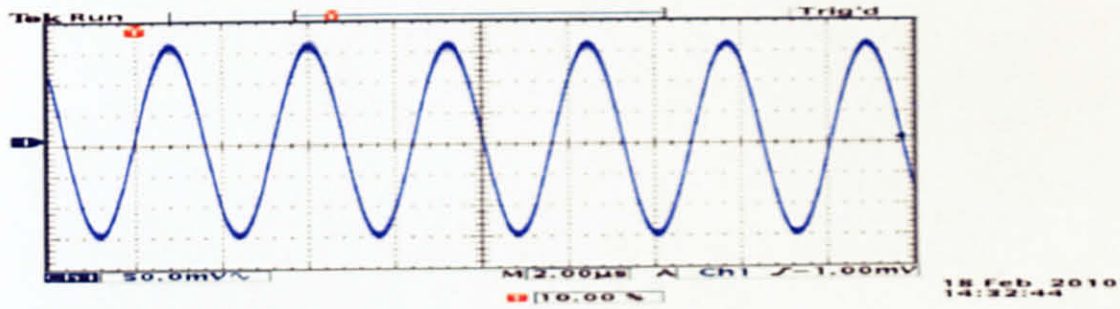

Figure 30 response at 400kHZ

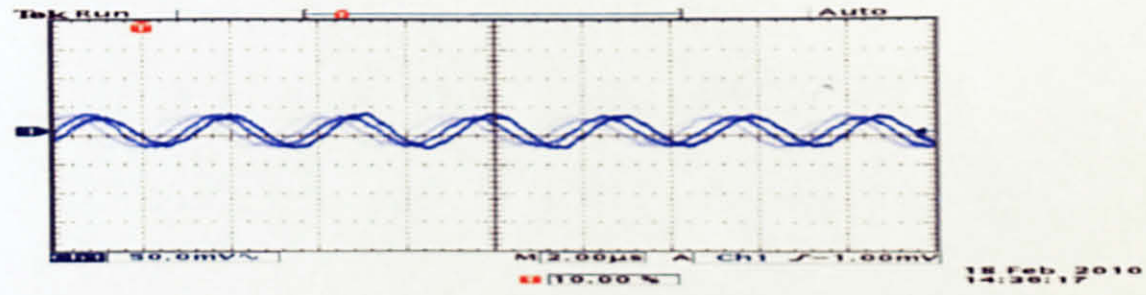

Figure 31 response at 420kHZ

4.1.4 Experiment #4 part 2 results: Decreased separation angle fluxgate setup.

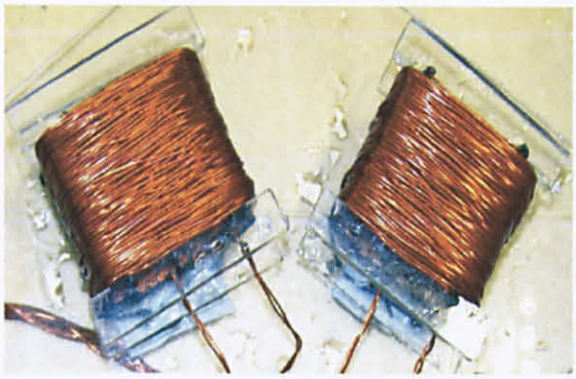

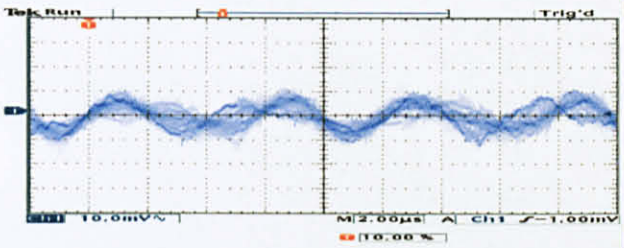

Figure 32 Response at 200 KHz

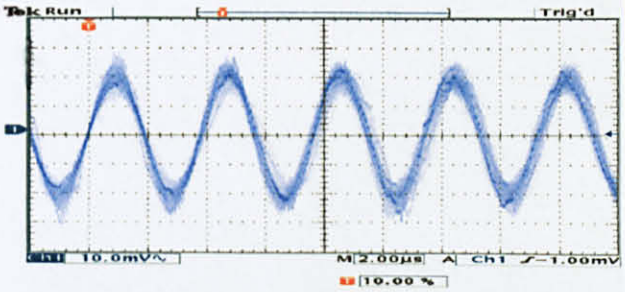

Figure 33 Response at 250 KHz

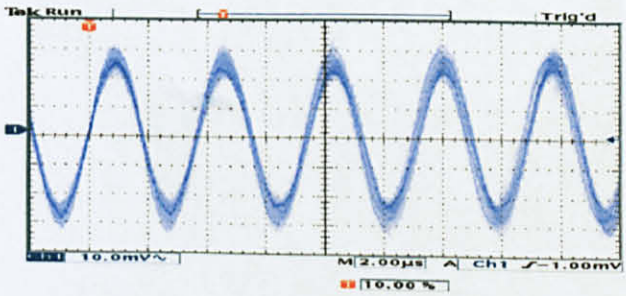

Figure 34 Response at 260 KHz

DISCUSSION

From figure 31 to figure 37 it is evident that when the fluxgates are placed next to each other with their separation angle decreased, the output response is lowered even more.

As it can be seen on the picture illustration on the left. There are two fluxgate units at an angle of 60 degrees with each other.

From this experiment we observed that the detector starts to detect the signal at frequencies as low as 200 KHz. The signal starts to be clear at around 250 KHz up to 280 KHz.

Figure 31 shows a sinusoidal signal but with a lot of noise.

This means that we have successfully lowered the frequency at this point. However the main objective has not been met yet (which is to lower the frequency to about 1 KHz).

The rest of the results have been illustrated on the next page.

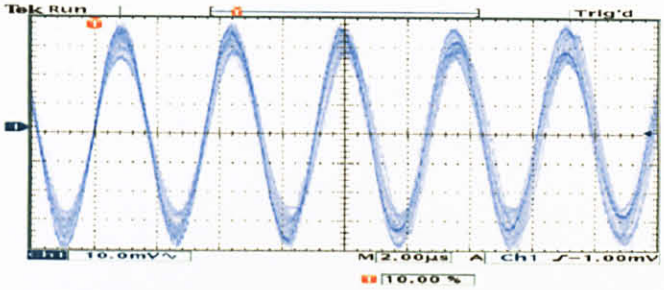

Figure 35 Response at 270 KHz

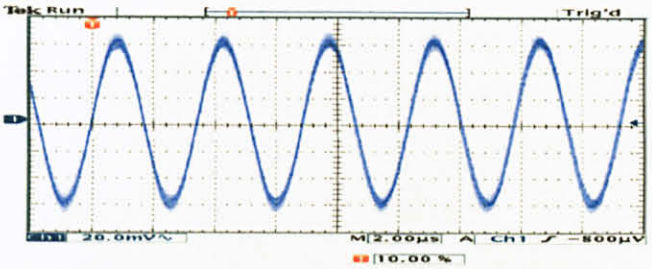

Figure 36 Response at 280 KHz

From these results, it is clear that our detector design will have to consist of more than two fluxgate units. And that these units must be at an angle with each other.

It is through these observations that it was decided to design and fabricate a detector that consists of six fluxgate units in a hexagon orientation.

The final prototype and test results of this new invention are illustrated and discussed on the next page.

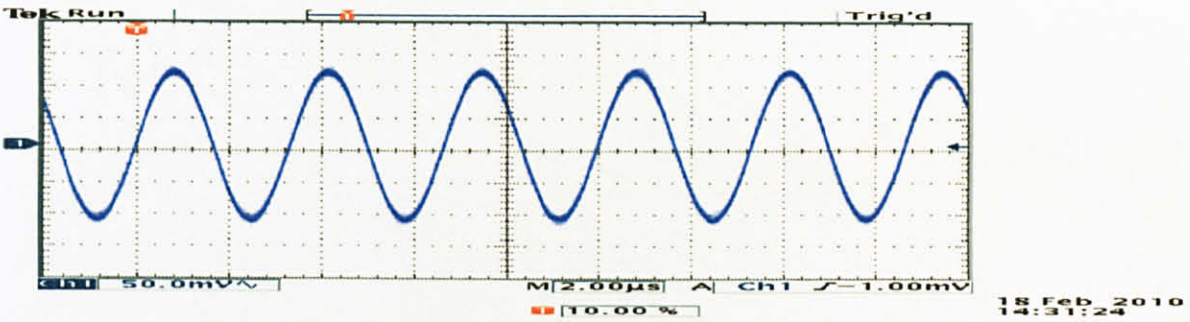

Figure 37 Response at 290 KHz

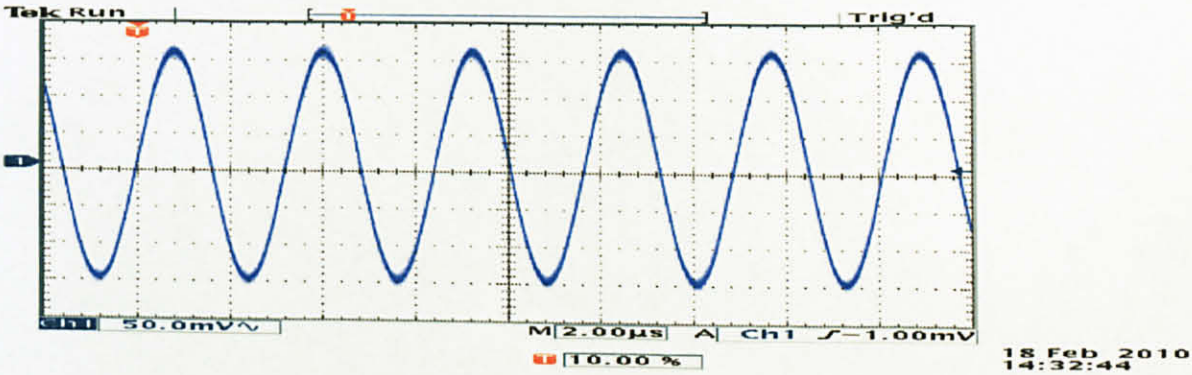

Figure 38 Response at 300 KHz

4.2 EM wave detector complete schematic and underwater test results

In section 3.8 (experiment 5), we tested the complete detector in salt-water.

The salt water had 1.18 Ωm conductivity. These are the results from this experiment.

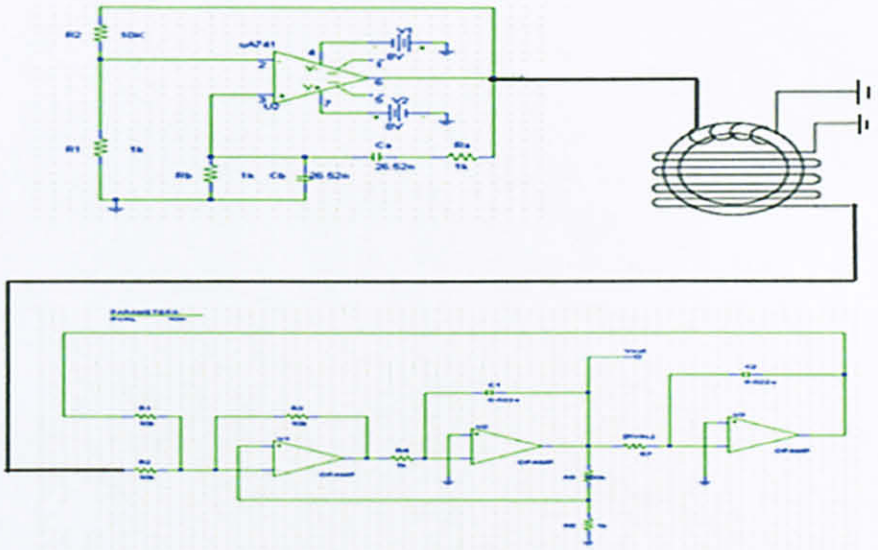

Figure 39 EM wave sensor full schematic

4.2.1 Experiment #5 results: Underwater test results at 1 KHz reception range

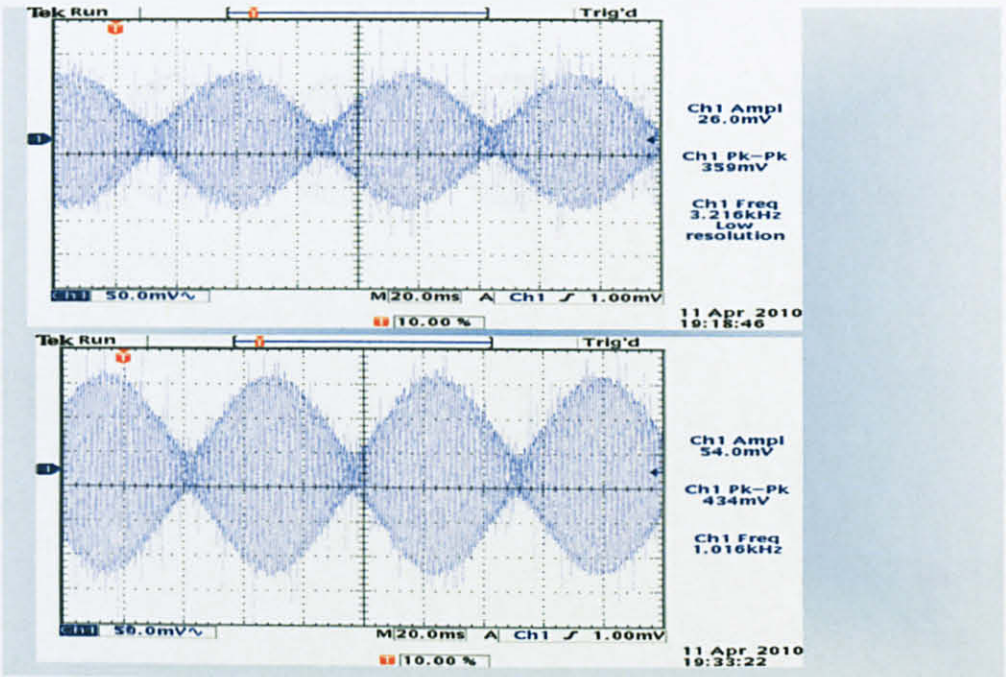

Figure 40 Results from the salt water test with 1 KHz frequency signal from the transmitter

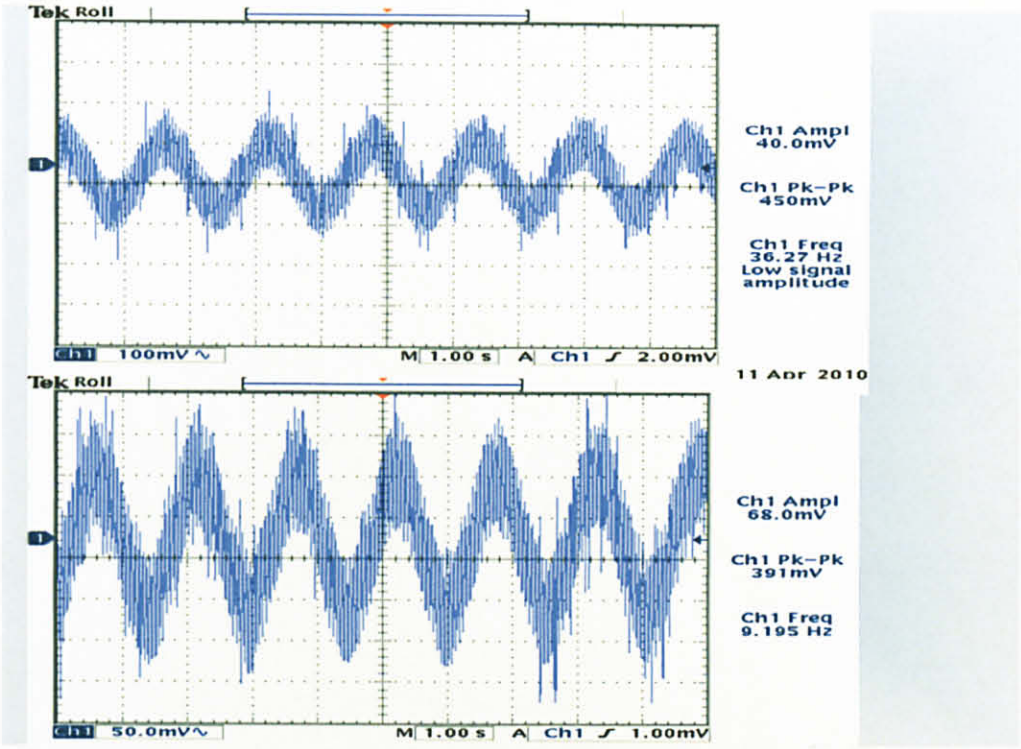

Figure 41 Underwater test results obtained via oscilloscope at frequencies lower than 1 KHz

From figure 40 we can see that the project's primary objective has been met since the detector was able to sense the signal at 1 KHz. This proves that our detector of hexagon shape is effective. Testing in salt water has also improved the results because of the increased conductivity.

In figure 41 we see the behavior of the detector when a signal lower than 1 KHz is received.

As we observed from experiment 1 and 2 that a single fluxgate was only most effective at a frequency of 1 MHz, and our new invention is effective at frequencies of 1 KHz and below because of the fluxgate orientation (hexagon), the optimum winding ratio (3:7) and the filter implementation with quality factor 33.7.

CHAPTER 5.
CONCLUSION AND RECOMMENDATIONS

5.1 Conclusion

1. The most effective turn ratio used was 3:7; with 62 drive winding and 145 sensor windings.
2. The hexagon design proved most effective when tested against other orientations.
3. The hexagon shape improved the sensitivity by up to 1000% as compared to using one fluxgate.
4. The design is also easy to implement and easy to manipulate, each fluxgate on the detector can be dismantled to function alone or replaced.
5. It is sensitive at frequencies as low as 1 KHz therefore can be used for seabed logging.
6. The filter implementation resulted to our design having a quality factor of 33.7
7. The bandwidth is 30 Hz when incoming signal is at 1 KHz.
8. The filter circuit uses the R_7 resistor instead of the R_4 resistor because it offers a stable amplitude on the output.

5.2 Recommendations

- For much improved efficiency our current hexagon detector can be designed to have a larger surface area.
- Nano- technology can be implemented on the detector.
- Advanced shielding can be implemented to eliminate the external unwanted noise due to the uncontrollable environmental aspects.

REFERENCES

[1] A. G Nekut, Brian R. Spies, February 1989. "Petroleum Exploration Using Controlled Source Electromagnetic Methods" *Proc* IEEE, Vol 77, No.2

[2] Fawwaz T. Ulaby, 'Electromagnetics for Engineers', ISBN 0 13 197064 X

[3] Prof Dr Noorhana Yahya "Seabed logging, a possible direct hydrocarbon detection for deep sea prospects using EM energy" by Prof Dr Noorhana Yahya; Universiti Teknologi Petronas.

[4] Eidesmo, T, S. Ellingsrud, L. M. MacGregor, S. Constable, M. C. Sinha, S. Johhanes, F. N. Kong "Seabedlogging, a new method for remote and direct identification of hydrocarbon filled layers in deepwater reas" First break, Vol. 20, 144-152, 2002.

[5] B. K. Bhattacharyya, 'Input Resistances of Horizontal Electric and Vertical Magnetic Dipoles Over a Homogenous Ground', IEEE Transactions on Antennas and Propagation May 1963.

[6] Slob, E. C. K. Wapenaar and R Sniedar, "Interferometry in dissipative media: Adressing the shallow sea problem for seabed logging applications" SEG expanded abstracts, Vol. 26,559-563, 2007

[7] Ronold W. P. King, 'Antennas in Material Media Near Boundaries with Application to Communication and Geophysical Exploration, Part I: The Bare Metal Dipole', IEEE Transactions on Antennas and Propagation, Vol. AP-34, No.4, April 1986.

[8] De Hop, A. T. "Handbook of radiation and scattering of waves, Academic press London, 1995.

[9] Vaage, S. T., J. T. Fokkemma and P. M. van der Berg, "Method for seismic exploration utilizing motion sensor and pressure sensor data" United States patent, No. 7123543, October 17, 2006.

[10] Fokkema, J. T. and P. M. van der Berg "Seismic applications of Acoustic Reciprocity" academic Press London, 1993.

[11] J.L. Brown. Jan. 1995. "High Sensitivity Magnetic Field Sensor Using GMR Materials with Integrated Electronics," *Proc* Symp on Circuits and Systems, Seattle, WA.

[12] R. Smith, A. Peter, "Using an induction coil sensor to indirectly measure the B-field response in the bandwidth of the transient electromagnetic method", *Exploration Geophysics* 30(4) 157 – 160. Csiro Publishing, 1999.

[13] P. Ripka. 1996. "Review of Fluxgate Sensors," *Sensors and Actuators* A, 33:129-141.

[14] 'Electromagnetic Waves' by The Open University http://openlearn.open.ac.uk

[15] J.M. Janicke. 1994. *The Magnetic Measurement Handbook*, New Jersey: Magnetic Research Press.

[16] J.E. Lenz. June 1990. "A Review of Magnetic Sensors," *Proc* IEEE, Vol. 78, No. 6:973- 989.

[17] E. Ramsden. Sept. 1994. "Measuring Magnetic Fields with Fluxgate Sensors," *Sensors*: 87- 90.

[18] B.B. Pant. Fall 1987. "Magneto resistive Sensors," *Scientific Honeyweller*, Vol. 8, No. 1:29-34.

[19] J.E. Lenz et al. 1992. "A Highly Sensitive Magnetoresistive Sensor," *Proc* Solid State Sensor and Actuator Workshop.

[20] 'Interference' from http://en.wikipedia.org/wiki/Interference Pearson Education, 2005.

[21] 'The Qualities and Advantages of Copper' from http://www.silmet.com

[22] David A. Hill, 'Magnetic Dipole Excitation of an Insulated Conductor of Finite Length', IEEE Transactions on Geo sciences and Remote Sensing, Vol. 28, No. 3, May 1990.

APPENDICES

APPENDIX A
SENSOR DETECTION RANGE

(adapted from: "Seabed logging, a possible direct hydrocarbon detection for deep sea prospects using EM energy" by Prof Dr Noorhana Yahya; Universiti Teknologi Petronas.)

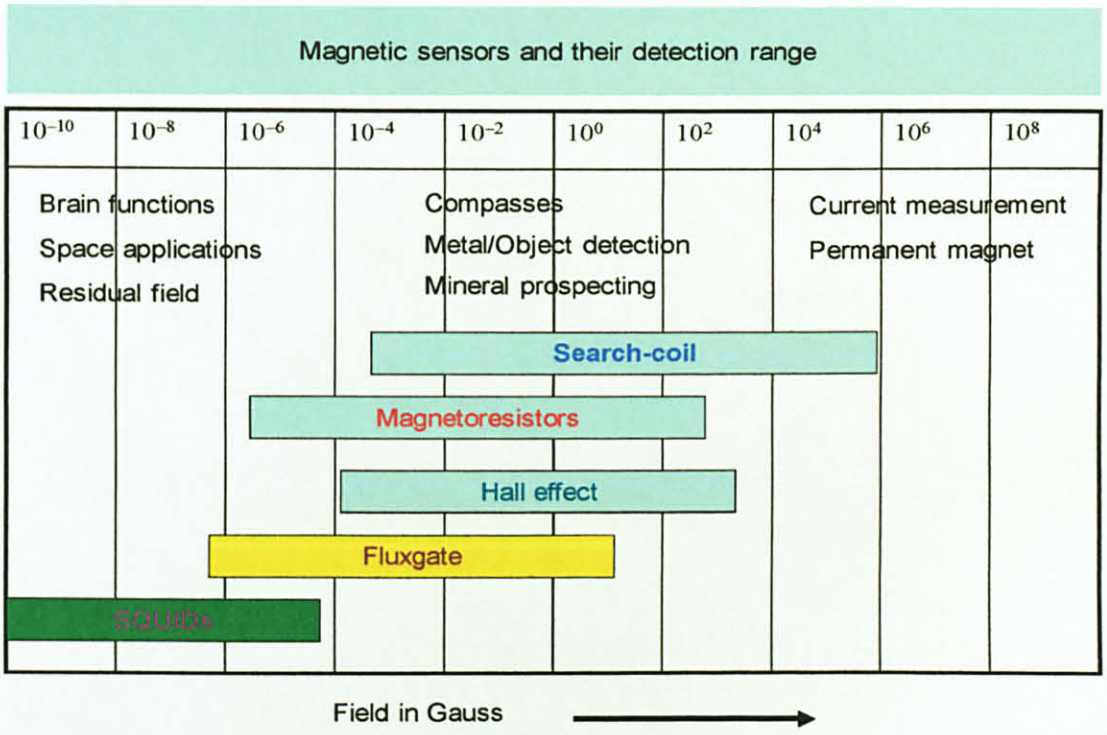

APPENDIX B

DATA SHEETS FOR CIRCUIT COMPONETS

National Semiconductor

August 2000

LM741
Operational Amplifier

General Description

The LM741 series are general purpose operational amplifiers which feature improved performance over industry standards like the LM709. They are direct, plug-in replacements for the 709C, LM201, MC1439 and 748 in most applications.

The amplifiers offer many features which make their application nearly foolproof: overload protection on the input and output, no latch-up when the common mode range is exceeded, as well as freedom from oscillations.

The LM741C is identical to the LM741/LM741A except that the LM741C has their performance guaranteed over a 0°C to +70°C temperature range, instead of −55°C to +125°C.

Features

Connection Diagrams

Metal Can Package

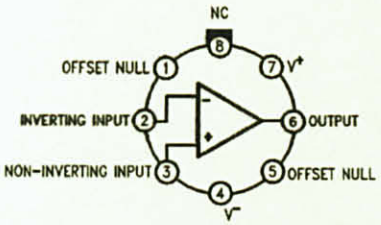

00934102

Note 1: LM741H is available per JM38510/10101

Order Number LM741H, LM741H/883 (Note 1), **LM741AH/883 or LM741CH**
See NS Package Number H08C

Dual-In-Line or S.O. Package

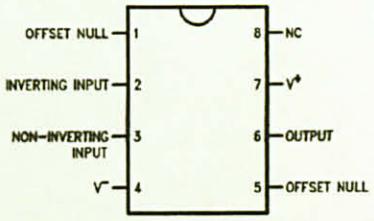

00934103

Order Number LM741J, LM741J/883, LM741CN
See NS Package Number J08A, M08A or N08E

Ceramic Flatpak

00934106

Order Number LM741W/883
See NS Package Number W10A

Typical Application

Offset Nulling Circuit

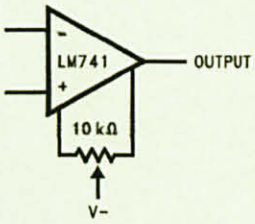

00934107

Absolute Maximum Ratings (Note 2)

If Military/Aerospace specified devices are required, please contact the National Semiconductor Sales Office/ Distributors for availability and specifications.

(Note 7)

	LM741A	LM741	LM741C
Supply Voltage	±22V	±22V	±18V
Power Dissipation (Note 3)	500 mW	500 mW	500 mW
Differential Input Voltage	±30V	±30V	±30V
Input Voltage (Note 4)	±15V	±15V	±15V
Output Short Circuit Duration	Continuous	Continuous	Continuous
Operating Temperature Range	−55°C to +125°C	−55°C to +125°C	0°C to +70°C
Storage Temperature Range	−65°C to +150°C	−65°C to +150°C	−65°C to +150°C
Junction Temperature	150°C	150°C	100°C
Soldering Information			
N-Package (10 seconds)	260°C	260°C	260°C
J- or H-Package (10 seconds)	300°C	300°C	300°C
M-Package			
Vapor Phase (60 seconds)	215°C	215°C	215°C
Infrared (15 seconds)	215°C	215°C	215°C
See AN-450 "Surface Mounting Methods and Their Effect on Product Reliability" for other methods of soldering surface mount devices.			
ESD Tolerance (Note 8)	400V	400V	400V

Electrical Characteristics (Note 5)

Parameter	Conditions	LM741A			LM741			LM741C			Units
		Min	Typ	Max	Min	Typ	Max	Min	Typ	Max	
Input Offset Voltage	$T_A = 25°C$										
	$R_S \le 10\ k\Omega$					1.0	5.0		2.0	6.0	mV
	$R_S \le 50\Omega$		0.8	3.0							mV
	$T_{AMIN} \le T_A \le T_{AMAX}$										
	$R_S \le 50\Omega$			4.0							mV
	$R_S \le 10\ k\Omega$						6.0			7.5	mV
Average Input Offset Voltage Drift				15							µV/°C
Input Offset Voltage Adjustment Range	$T_A = 25°C$, $V_S = \pm 20V$	±10				±15			±15		mV
Input Offset Current	$T_A = 25°C$		3.0	30		20	200		20	200	nA
	$T_{AMIN} \le T_A \le T_{AMAX}$			70		85	500			300	nA
Average Input Offset Current Drift				0.5							nA/°C
Input Bias Current	$T_A = 25°C$		30	80		80	500		80	500	nA
	$T_{AMIN} \le T_A \le T_{AMAX}$			0.210			1.5			0.8	µA
Input Resistance	$T_A = 25°C$, $V_S = \pm 20V$	1.0	6.0		0.3	2.0		0.3	2.0		MΩ
	$T_{AMIN} \le T_A \le T_{AMAX}$, $V_S = \pm 20V$	0.5									MΩ
Input Voltage Range	$T_A = 25°C$							±12	±13		V
	$T_{AMIN} \le T_A \le T_{AMAX}$				±12	±13					V

Electrical Characteristics (Note 5) (Continued)

Parameter	Conditions	LM741A			LM741			LM741C			Units
		Min	Typ	Max	Min	Typ	Max	Min	Typ	Max	
Large Signal Voltage Gain	$T_A = 25°C$, $R_L \geq 2\ k\Omega$										
	$V_S = \pm 20V$, $V_O = \pm 15V$	50									V/mV
	$V_S = \pm 15V$, $V_O = \pm 10V$				50	200		20	200		V/mV
	$T_{AMIN} \leq T_A \leq T_{AMAX}$, $R_L \geq 2\ k\Omega$,										
	$V_S = \pm 20V$, $V_O = \pm 15V$	32									V/mV
	$V_S = \pm 15V$, $V_O = \pm 10V$				25			15			V/mV
	$V_S = \pm 5V$, $V_O = \pm 2V$	10									V/mV
Output Voltage Swing	$V_S = \pm 20V$										
	$R_L \geq 10\ k\Omega$	±16									V
	$R_L \geq 2\ k\Omega$	±15									V
	$V_S = \pm 15V$										
	$R_L \geq 10\ k\Omega$				±12	±14		±12	±14		V
	$R_L \geq 2\ k\Omega$				±10	±13		±10	±13		V
Output Short Circuit Current	$T_A = 25°C$	10	25	35		25			25		mA
	$T_{AMIN} \leq T_A \leq T_{AMAX}$	10		40							mA
Common-Mode Rejection Ratio	$T_{AMIN} \leq T_A \leq T_{AMAX}$										
	$R_S \leq 10\ k\Omega$, $V_{CM} = \pm 12V$				70	90		70	90		dB
	$R_S \leq 50\Omega$, $V_{CM} = \pm 12V$	80	95								dB
Supply Voltage Rejection Ratio	$T_{AMIN} \leq T_A \leq T_{AMAX}$, $V_S = \pm 20V$ to $V_S = \pm 5V$										
	$R_S \leq 50\Omega$	86	96								dB
	$R_S \leq 10\ k\Omega$				77	96		77	96		dB
Transient Response	$T_A = 25°C$, Unity Gain										
Rise Time			0.25	0.8		0.3			0.3		µs
Overshoot			6.0	20		5			5		%
Bandwidth (Note 6)	$T_A = 25°C$	0.437	1.5								MHz
Slew Rate	$T_A = 25°C$, Unity Gain	0.3	0.7			0.5			0.5		V/µs
Supply Current	$T_A = 25°C$					1.7	2.8		1.7	2.8	mA
Power Consumption	$T_A = 25°C$										
	$V_S = \pm 20V$		80	150							mW
	$V_S = \pm 15V$					50	85		50	85	mW
LM741A	$V_S = \pm 20V$										
	$T_A = T_{AMIN}$			165							mW
	$T_A = T_{AMAX}$			135							mW
LM741	$V_S = \pm 15V$										
	$T_A = T_{AMIN}$					60	100				mW
	$T_A = T_{AMAX}$					45	75				mW

Note 2: "Absolute Maximum Ratings" indicate limits beyond which damage to the device may occur. Operating Ratings indicate conditions for which the device is functional, but do not guarantee specific performance limits.

Electrical Characteristics (Note 5) (Continued)

Note 3: For operation at elevated temperatures, these devices must be derated based on thermal resistance, and T_j max. (listed under "Absolute Maximum Ratings"). $T_j = T_A + (\theta_{jA} P_D)$.

Thermal Resistance	Cerdip (J)	DIP (N)	HO8 (H)	SO-8 (M)
θ_{jA} (Junction to Ambient)	100°C/W	100°C/W	170°C/W	195°C/W
θ_{jC} (Junction to Case)	N/A	N/A	25°C/W	N/A

Note 4: For supply voltages less than ±15V, the absolute maximum input voltage is equal to the supply voltage.

Note 5: Unless otherwise specified, these specifications apply for V_S = ±15V, −55°C ≤ T_A ≤ +125°C (LM741/LM741A). For the LM741C/LM741E, these specifications are limited to 0°C ≤ T_A ≤ +70°C.

Note 6: Calculated value from: BW (MHz) = 0.35/Rise Time(μs).

Note 7: For military specifications see RETS741X for LM741 and RETS741AX for LM741A.

Note 8: Human body model, 1.5 kΩ in series with 100 pF.

Schematic Diagram

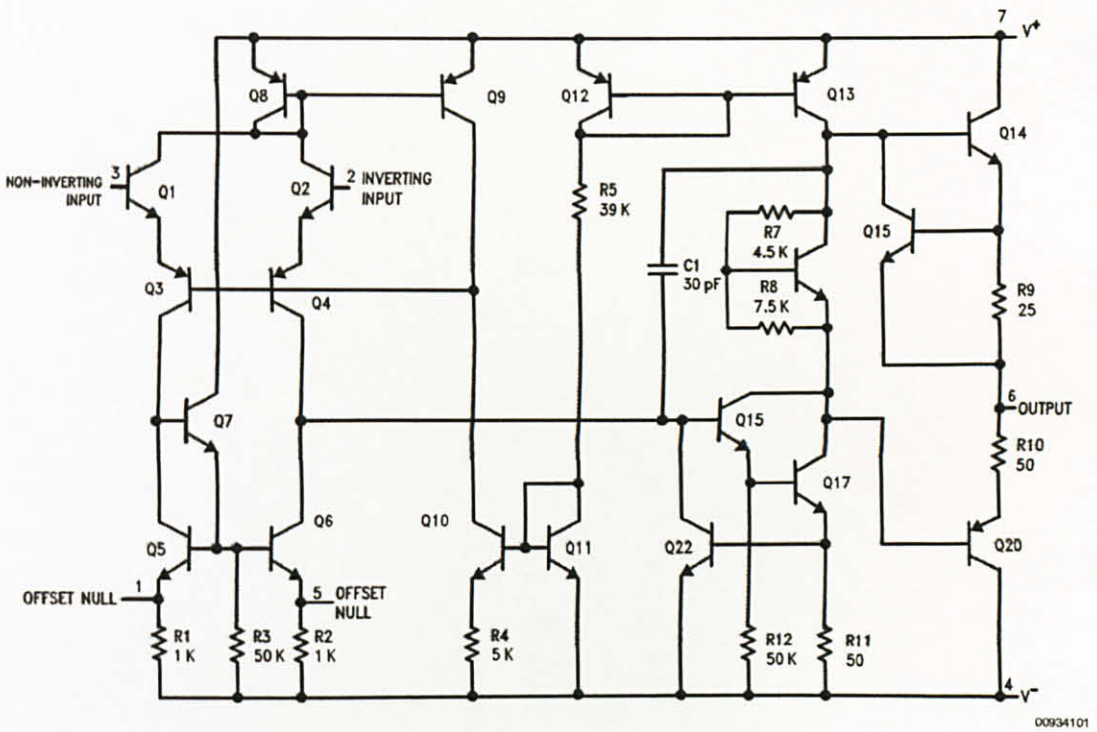

Physical Dimensions inches (millimeters)
unless otherwise noted

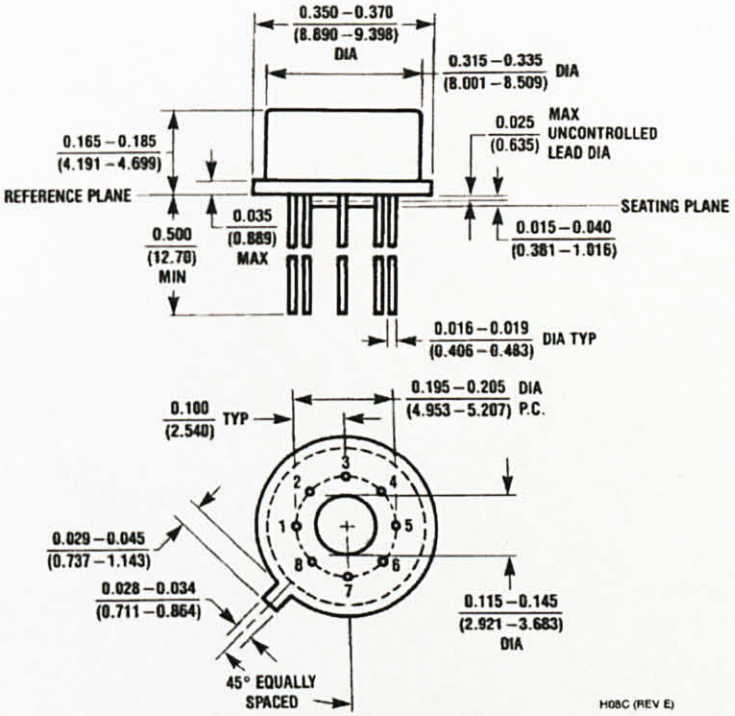

Metal Can Package (H)
Order Number LM741H, LM741H/883, LM741AH/883, LM741AH-MIL or LM741CH
NS Package Number H08C

Physical Dimensions inches (millimeters) unless otherwise noted (Continued)

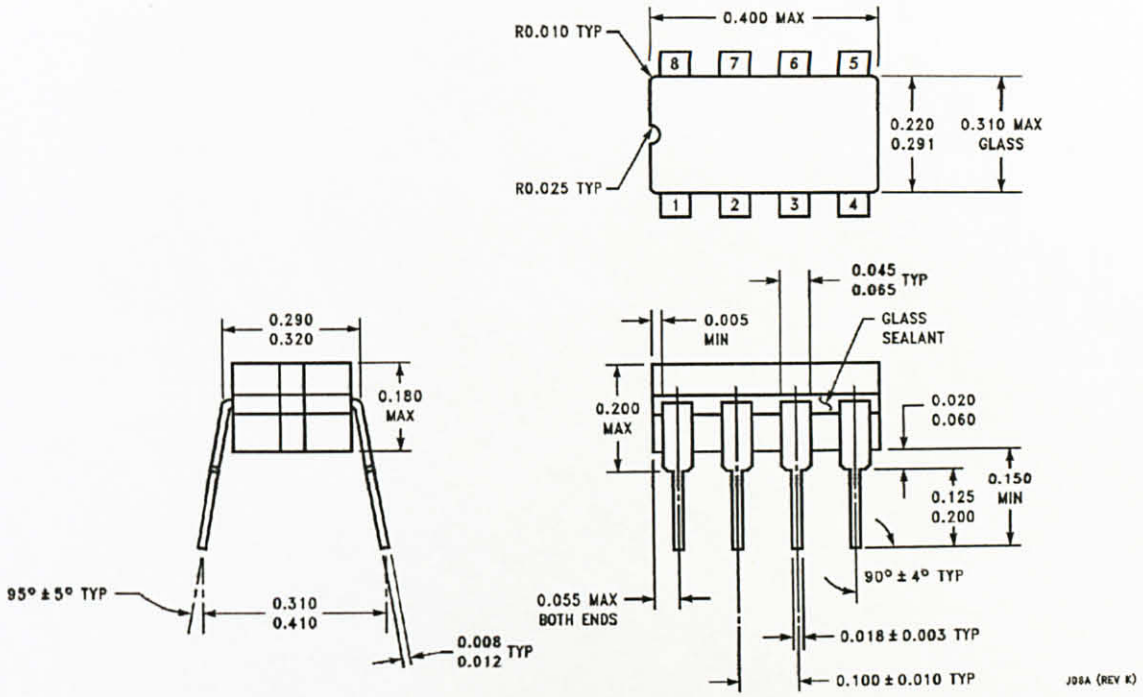

Ceramic Dual-In-Line Package (J)
Order Number LM741J/883
NS Package Number J08A

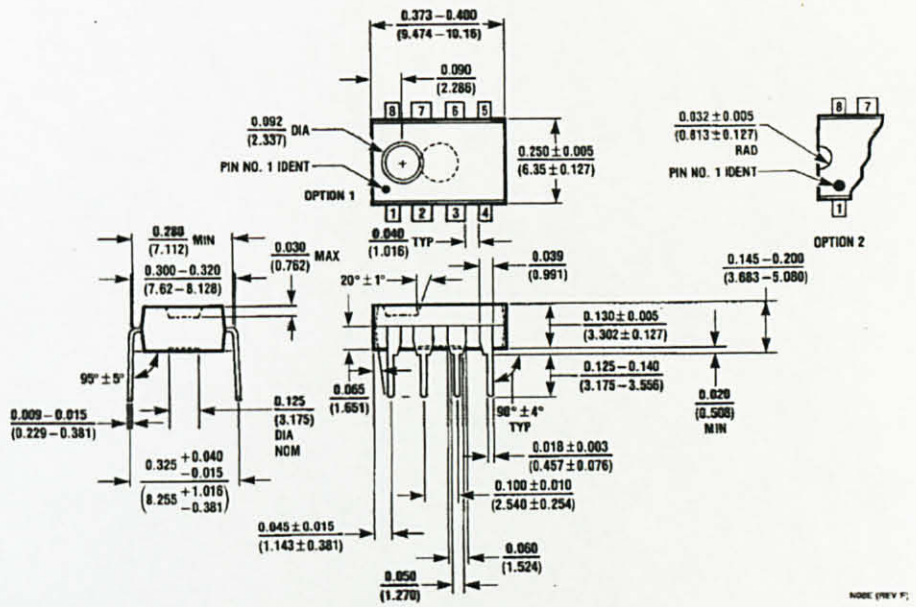

Dual-In-Line Package (N)
Order Number LM741CN
NS Package Number N08E

Physical Dimensions inches (millimeters) unless otherwise noted (Continued)

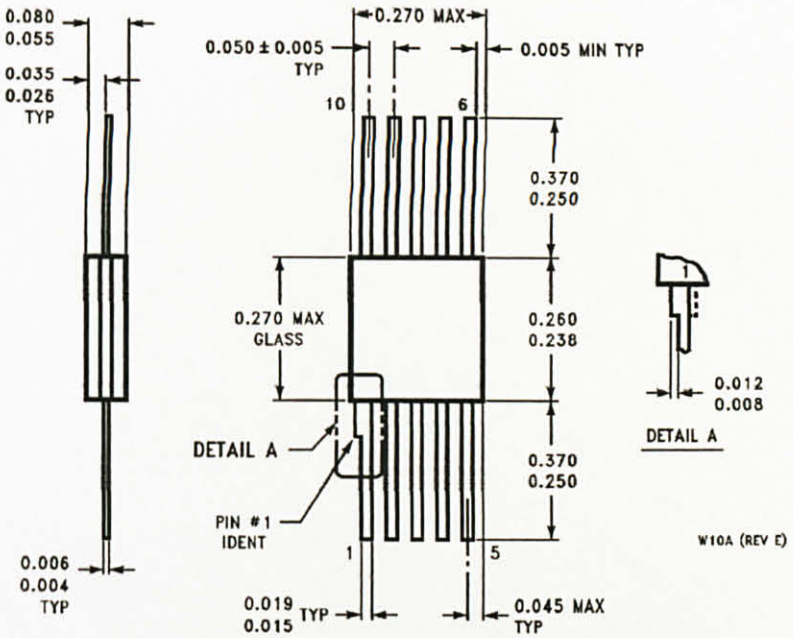

10-Lead Ceramic Flatpak (W)
Order Number LM741W/883, LM741WG-MPR or LM741WG/883
NS Package Number W10A

National Semiconductor
Americas Customer
Support Center
Email: new.feedback@nsc.com
Tel: 1-800-272-9959

www.national.com

National Semiconductor
Europe Customer Support Center
Fax: +49 (0) 180-530 85 86
Email: europe.support@nsc.com
Deutsch Tel: +49 (0) 69 9508 6208
English Tel: +44 (0) 870 24 0 2171
Français Tel: +33 (0) 1 41 91 8790

National Semiconductor
Asia Pacific Customer
Support Center
Email: ap.support@nsc.com

National Semiconductor
Japan Customer Support Center
Fax: 81-3-5639-7507
Email: jpn.feedback@nsc.com
Tel: 81-3-5639-7560

SGS-THOMSON MICROELECTRONICS

UA741

GENERAL-PURPOSE SINGLE OP-AMPs

- LARGE INPUT VOLTAGE RANGE
- NO LATCH-UP
- HIGH GAIN
- SHORT-CIRCUIT PROTECTION
- NO FREQUENCY COMPENSATION REQUIRED
- SAME PIN CONFIGURATION AS THE UA709

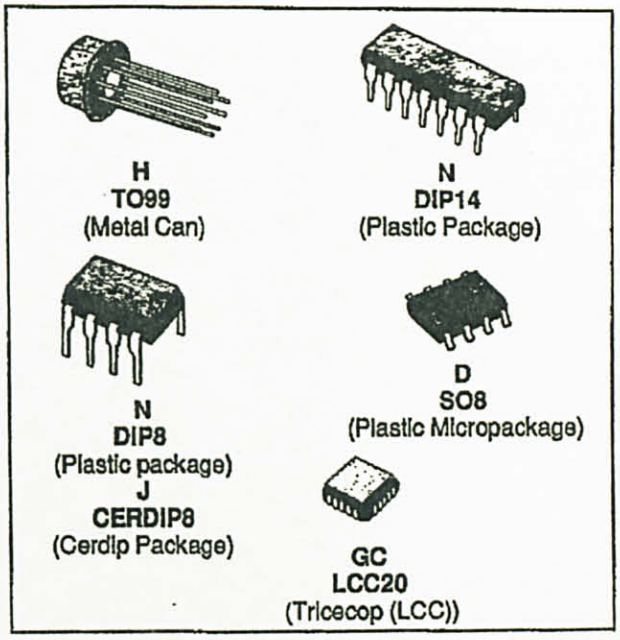

H
TO99
(Metal Can)

N
DIP14
(Plastic Package)

N
DIP8
(Plastic package)

D
SO8
(Plastic Micropackage)

J
CERDIP8
(Cerdip Package)

GC
LCC20
(Tricecop (LCC))

DESCRIPTION

The UA741 is a high performance monolithic operational constructed on a single silicon chip. It is intended for a wide range of analog applications.

- Summing amplifier
- Voltage follower
- Integrator
- Active filter
- Function generator.

The high gain and wide range of operating voltages provides superior performance integrator, summing amplifier, and general feedback applications. the internal compensation network (6 dB/octave) insures stability in closed loop applications.

ORDER CODES

Part Number	Temperature Range	Package					
		H	J	GC	N	N 14	D
UA741C/E	0 °C to + 70 °C	•	•		•	•	•
UA741I	–40 °C to + 105 °C	•			•	•	
UA741M/A	–55 °C to + 125 °C	•	•	•			

Note : HI-Rel Versions Available
Examples : UA741CN, UA741IH

PIN CONNECTIONS (top views)

DIP8/CERDIP8 SO8

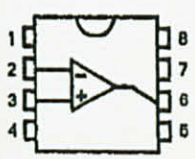

1 - Offset null
2 - Inverting Input
3 - Non-Inverting Input
4 - V_{cc}^-

TO99

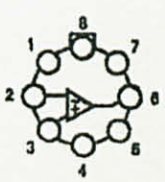

5 - Offset null
6 - Output
7 - V_{cc}^+
8 - NC

LCC20

1 - NC
2 - Offset null
3 - NC
4 - NC
5 - Inverting Input
6 - NC
7 - Non-Inverting Input
8 - NC
9 - NC
11 - NC
12 - Offset null
13 - NC
14 - NC
15 - Output
16 - NC
17 - V_{cc}^+
18 - NC
19 - NC
20 - NC

DIP14

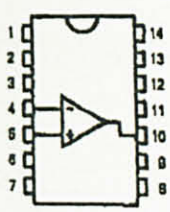

1 - NC
2 - NC
3 - Offset null
4 - Inverting Input
5 - Non-Inverting Input
6 - V_{cc}^-
7 - NC
8 - NC
9 - Offset null
10 - Output
11 - V_{cc}^+
12 - NC
13 - NC
14 - NC

ABSOLUTE MAXIMUM RATINGS S G S-THOMSON 30E D

Symbol	Parameter	Value			Unit
		UA741M, A	UA741I	UA741C, E	
V_{cc}	Supply Voltage	± 22	± 22	± 22	V
V_i	Input Voltage	± 15	± 15	± 15	V
V_{id}	Differential Input Voltage	± 30	± 30	± 30	V
P_{tot}	Power Dissipation	500	500	500	mW
	Output Short-circuit Duration	Infinite			
T_{oper}	Operating Free-air Temperature Range	– 55 to + 125	– 40 to + 105	0 to + 70	°C
T_{stg}	Storage Temperature Range	– 65 to 150	– 65 to 150	– 65 to 150	°C

SCHEMATIC DIAGRAM

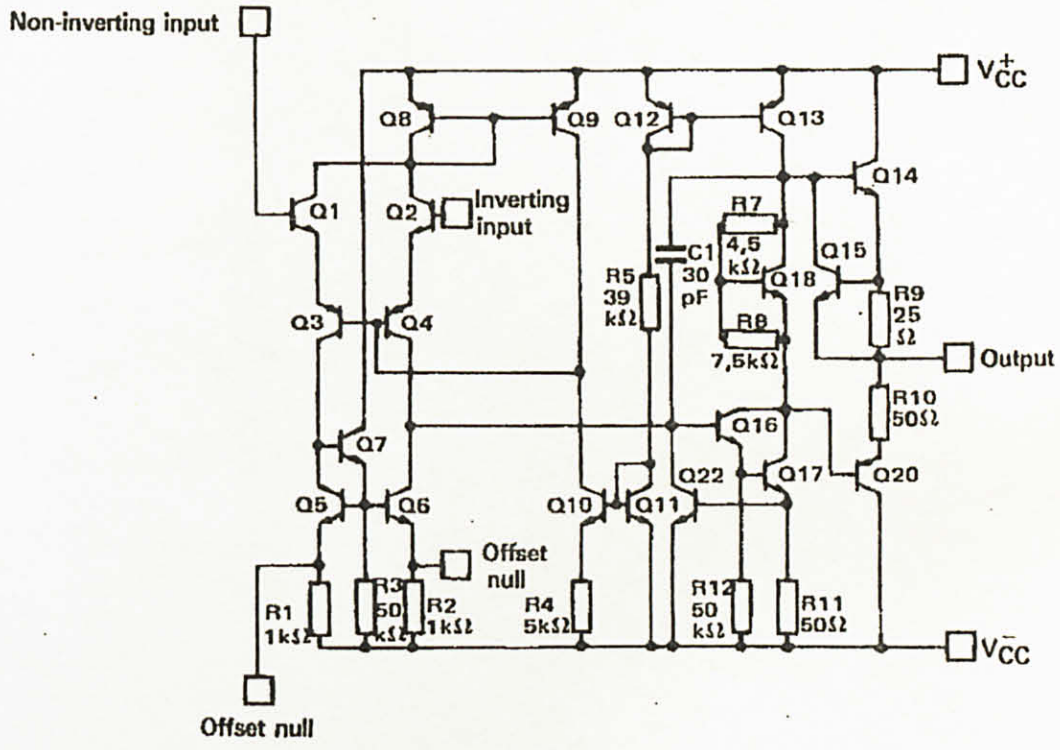

Case	Offset Null	Inverting Input	Non-Inverting Input	V_{cc}^-	V_{cc}^+	Output	N.C.
TO99/DIP8/CERDIP8/SO8	1, 5	2	3	4	7	6	8
DIP14	3, 9	4	5	6	11	10	*
LCC20	2, 12	5	7	10	17	15	*

* TO116, LCC20 : Other pins are not connected.

ELECTRICAL CHARACTERISTICS

UA741M/A : $-55\ °C \le T_{amb} \le +125\ °C$, $V_{CC} = \pm 15\ V$
UA741I : $-40\ °C \le T_{amb} \le +105\ °C$, $V_{CC} = \pm 15\ V$
UA741C/E : $0\ °C \le T_{amb} \le +70\ °C$, $V_{CC} = \pm 15\ V$
(unless otherwise specified)

Symbol	Parameter	UA741C, E, I, M, A			Unit
		Min.	Typ.	Max.	
V_{IO}	Input Offset Voltage $R_S \le 10\ k\Omega$ $T_{amb} = 25\ °C$ $T_{min} \le T_{amb} \le T_{max}$ UA741E, A $T_{amb} = 25\ °C$ $T_{min} \le T_{amb} \le T_{max}$		1 1	5 6 2 4	mV
I_{IO}	Input Offset Current $T_{amb} = 25\ °C$ $T_{min} \le T_{amb} \le T_{max}$		2	20 40	nA
I_{IB}	Input Bias Current $T_{amb} = 25\ °C$ $T_{min} \le T_{amb} \le T_{max}$		10	100 200	nA
A_{VD}	Large Signal Voltage Gain ($V_O = \pm 10\ V$, $R_L = 2\ k\Omega$) $T_{amb} = 25\ °C$ $T_{min} \le T_{amb} \le T_{max}$	 50 25	 200		V/mV
SVR	Supply Voltage Rejection Ratio ($R_S \le 10\ k\Omega$) $T_{amb} = 25\ °C$ $T_{min} \le T_{amb} \le T_{max}$	 77 77	 90		dB
I_{CC}	Supply Current, no Load $T_{amb} = 25\ °C$ $T_{min} \le T_{amb} \le T_{max}$		1.7	2.8 3.3	mA
V_I	Input Voltage Range $T_{amb} = 25\ °C$ $T_{min} \le T_{amb} \le T_{max}$	 -12 -12		 $+12$ $+12$	V
CMR	Common Mode Rejection Ratio ($R_S \le 10\ k\Omega$) $T_{amb} = 25\ °C$ $T_{min} \le T_{amb} \le T_{max}$	 70 70	 90		dB
I_{OS}	Output Short-circuit Current $T_{amb} = 25\ °C$	10	25	40	mA
$\pm V_{OPP}$	Output Voltage Swing $T_{amb} = 25\ °C$ $R_L = 10\ k\Omega$ $R_L = 2\ k\Omega$ $T_{min} \le T_{amb} \le T_{max}$ $R_L = 10\ k\Omega$ $R_L = 2\ k\Omega$	 12 10 12 10	 14 13		V
S_{VO}	Slew-rate ($V_I = \pm 10\ V$, $R_L = 2\ k\Omega$ $C_L \le 100\ pF$, $T_{amb} = 25\ °C$, unity gain)	0.25	0.5		V/µs
t_r	Rise Time ($V_I = \pm 20\ mV$, $R_L = 2\ k\Omega$, $C_L \le 100\ pF$ $T_{amb} = 25\ °C$, unity gain)		0.3		µs
K_{OV}	Overshoot ($V_I = \pm 20\ mV$, $R_L = 2\ k\Omega$, $C_L \le 100\ pF$, $T_{amb} = 25\ °C$, unity gain)		5		%
R_I	Input Resistance, $T_{amb} = 25\ °C$	0.3	2		mΩ

ELECTRICAL CHARACTERISTICS (continued)

Symbol	Parameter	UA741C, E, I, M, A			Unit
		Min.	Typ.	Max.	
GPB	Gain Bandwidth Product (V_I = 10 mV, R_L = 2 kΩ, $C_L \leq$ 100 pF f = 100 kHz, T_{amb} = 25 °C)	0.7	1	1.6	MHz
THD	Total Harmonic Distortion (f = 1 kHz, A_V = 20 dB, R_L 2 kΩ, V_O = 2 V_{pp} $C_L \leq$ 100 pF, T_{amb} = 25 °C)		0.06		%
V_N	Equivalent Input Noise Voltage (f = 1 kHz, R_G = 100 Ω)		23		nV/√Hz
	Phase Margin		50		Degrees

OPEN LOOP VOLTAGE GAIN (Typ.)

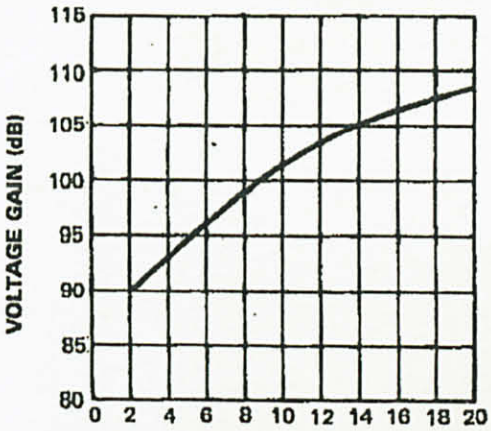

E88UA741-02

OPEN LOOP FREQUENCY RESPONSE (Typ.)

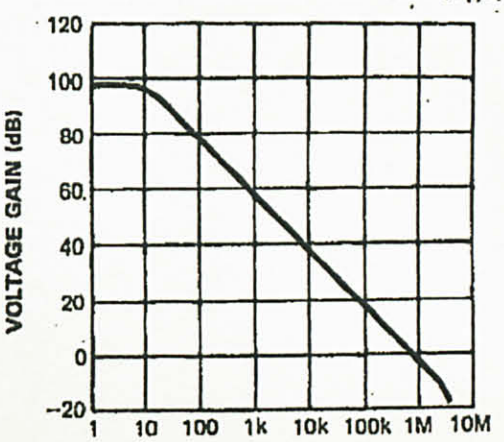

E88UA741-03

TRANSIENT RESPONSE (Typ.)

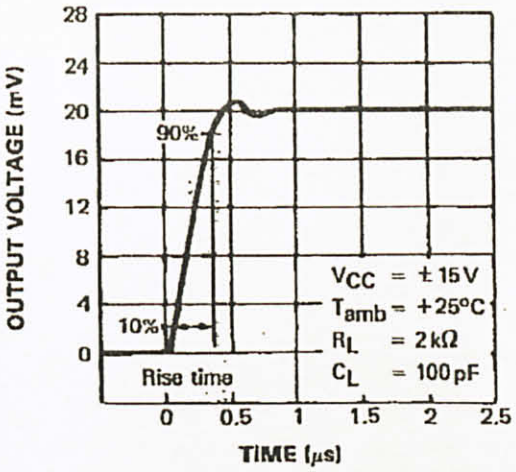

E88UA741-04

ABSOLUTE MAXIMUM POWER DISSIPATION

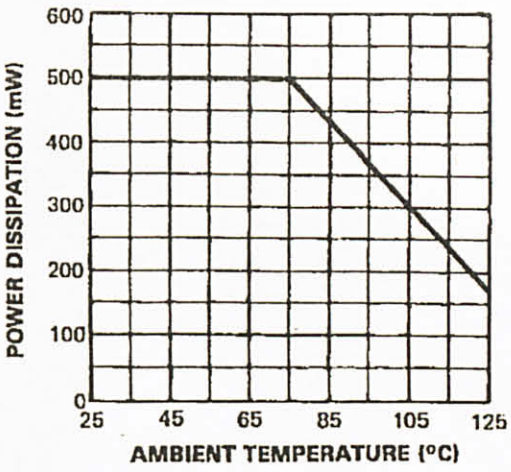

E88UA741-05

OUTPUT VOLTAGE SWING

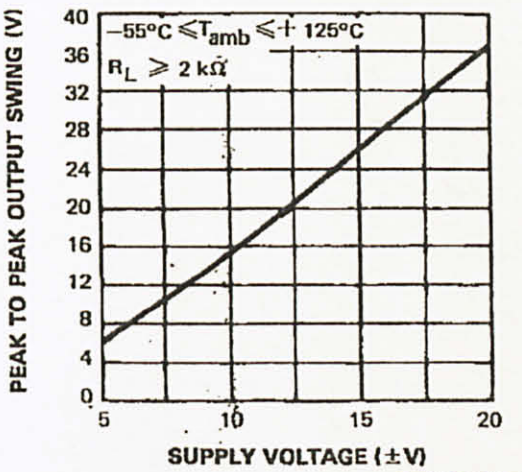

E88UA741-06

INPUT COMMON MODE VOLTAGE RANGE

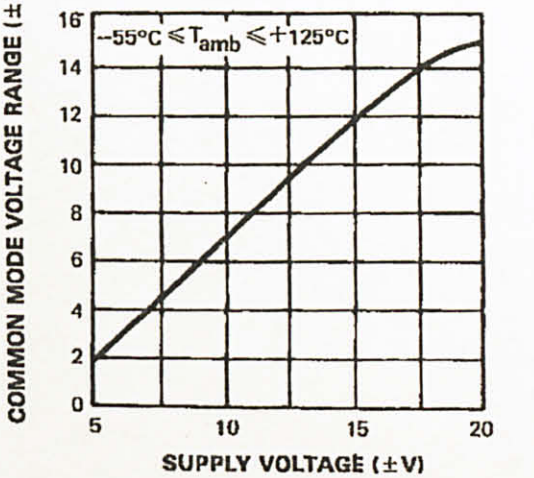

E88UA741-07

POWER CONSUMPTION

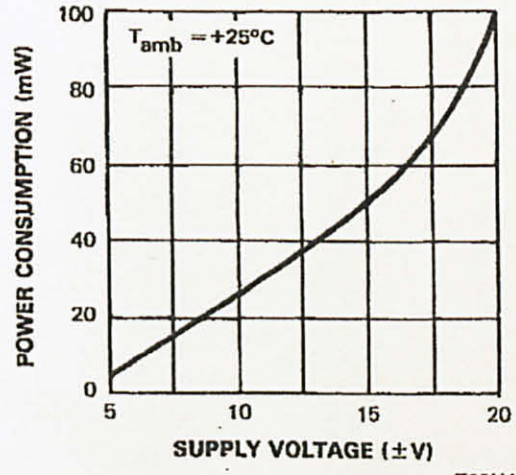

E88UA741-08

OUTPUT CURRENT vs AMBIENT TEMPERATURE

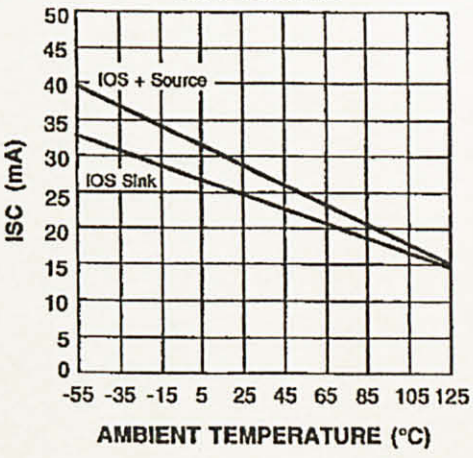

E88UA741-09

OUTPUT VOLTAGE SWING

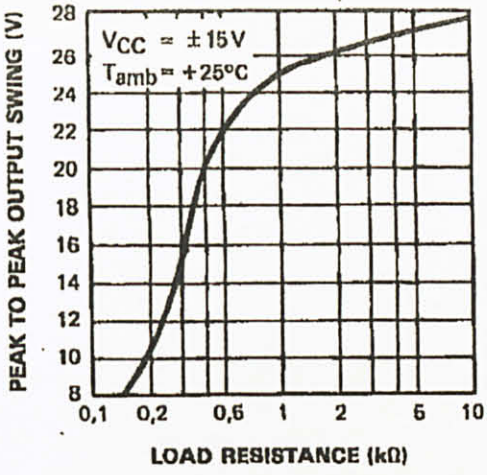

E88UA741-10

OUTPUT VOLTAGE SWING

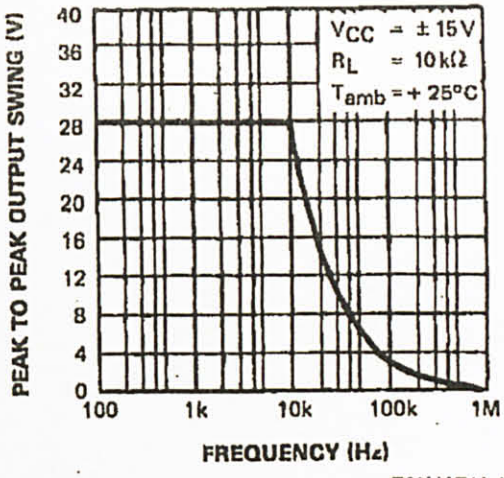

E88UA741-11

EQUIVALENT INPUT NOISE vs FREQUENCY

Rg = 100 Ω

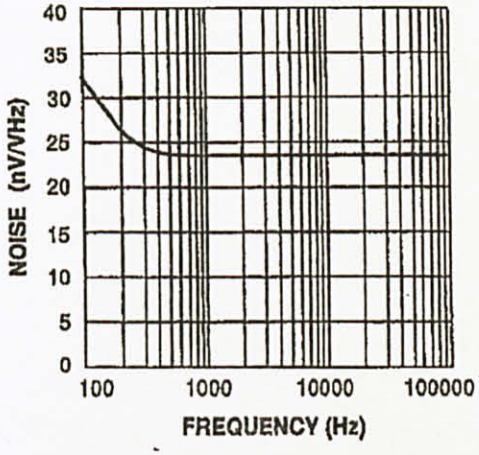

E88UA741-12

INPUT NOISE CURRENT

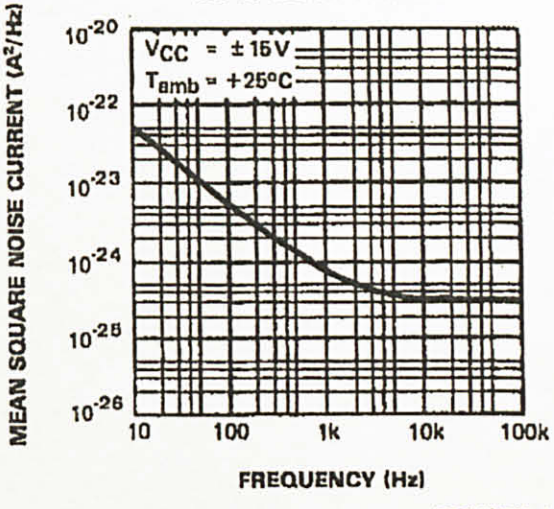

E88UA741-13

EQUIVALENT INPUT NOISE vs AMBIENT TEMPERATURE

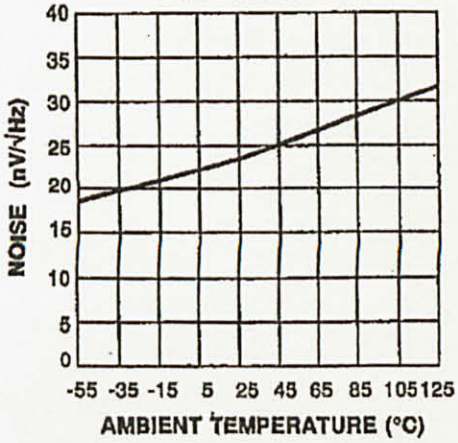

E88UA741-14

LARGE SIGNAL VOLTAGE GAIN vs AMBIENT TEMPERATURE

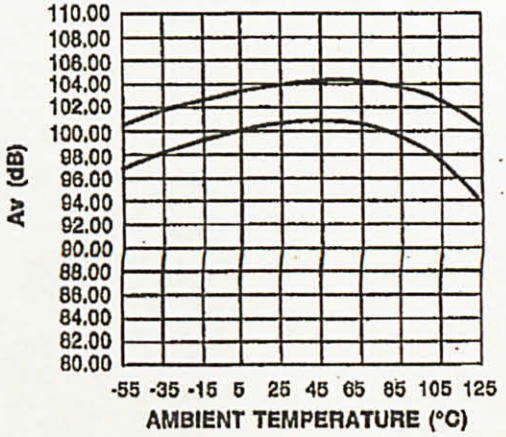

E88UA741-15

GAIN BANDWIDTH PRODUCT vs AMBIENT TEMPERATURE

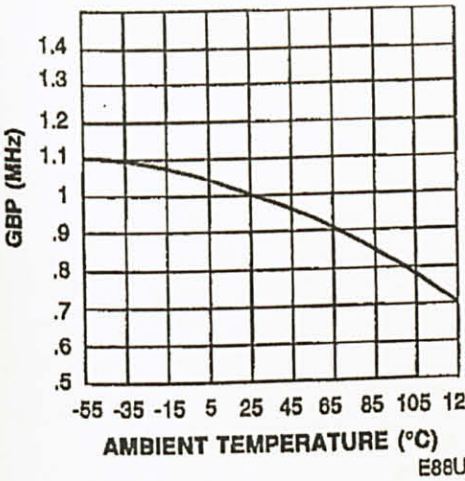

E88UA741-16

POWER SUPPLY & COMMON MODE REJECTION RATIO vs AMBIENT TEMPERATURE

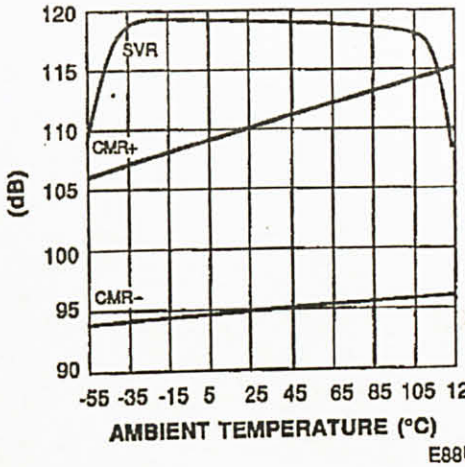

E88UA741-17

INPUT BIAS CURRENT vs AMBIENT TEMPERATURE

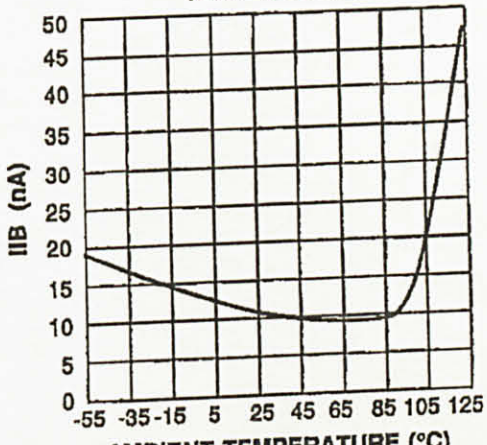

E88UA741-18

MEASUREMENT DIAGRAMS

S G S-THOMSON 30E D

VOLTAGE OFFSET NULL CIRCUIT

TO99 – DIP8 – CERDIP8

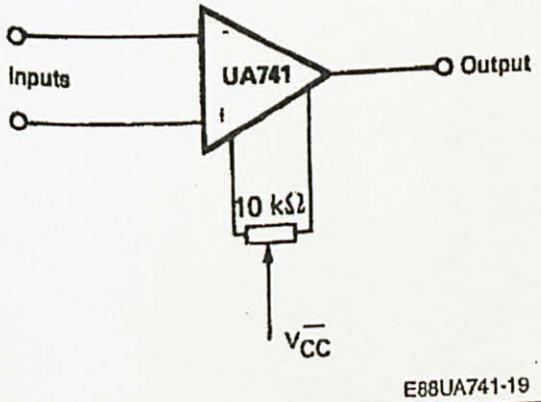

E88UA741-19

TRANSIENT RESPONSE TEST CIRCUIT

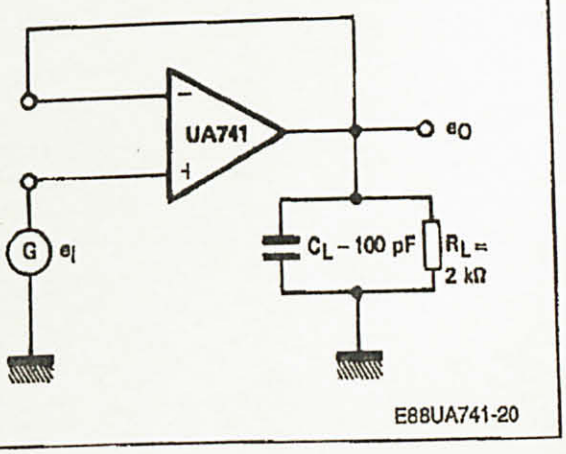

E88UA741-20

MEASUREMENT DIAGRAMS (continued)

CURRENT TO VOLTAGE CONVERTER

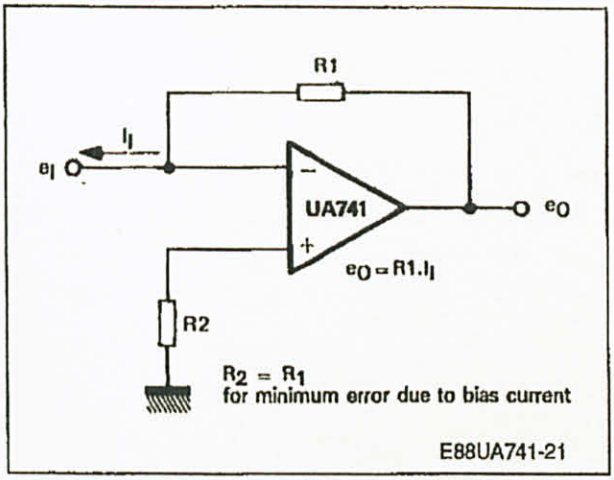

NEUTRALIZING INPUT CAPACITANCE TO OPTIMIZE RESPONSE TIME

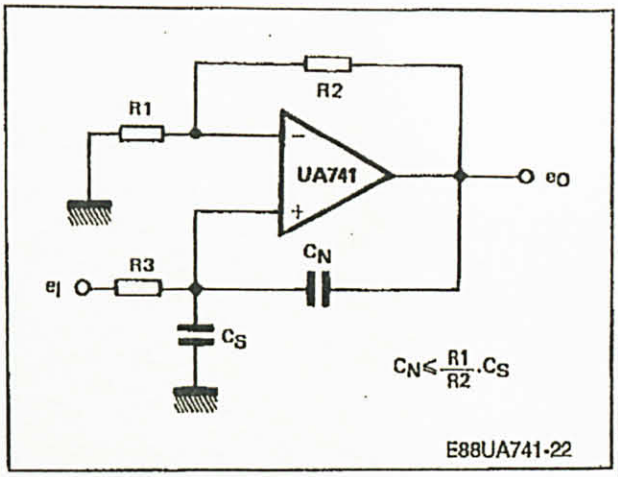

POSITIVE VOLTAGE REFERENCE

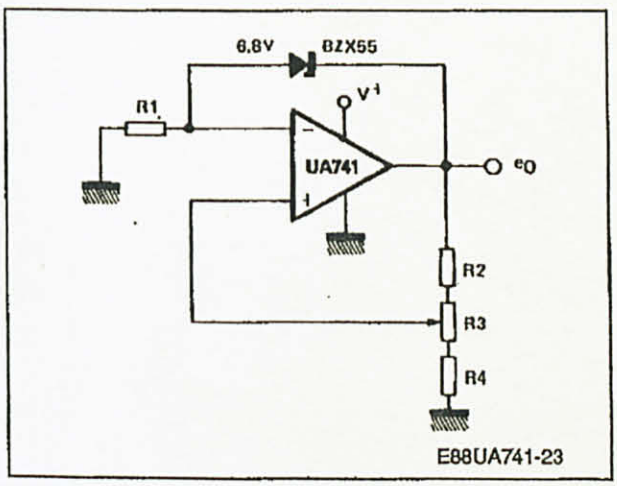

NEGATIVE VOLTAGE REFERENCE

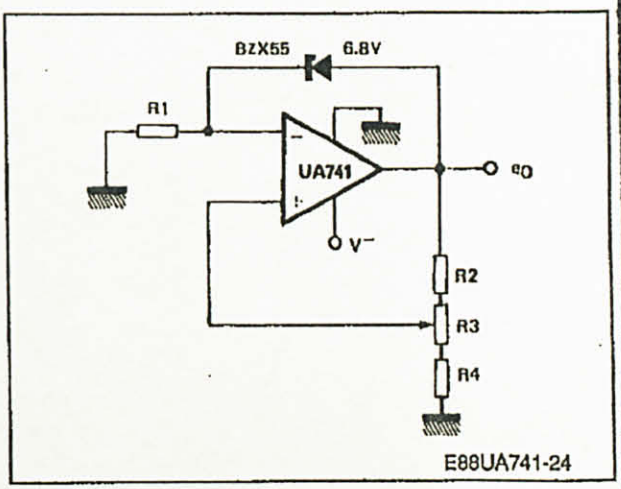

S G S-THOMSON 30E D

PACKAGE MECHANICAL DATA

8 PINS – TO99 – METAL CAN

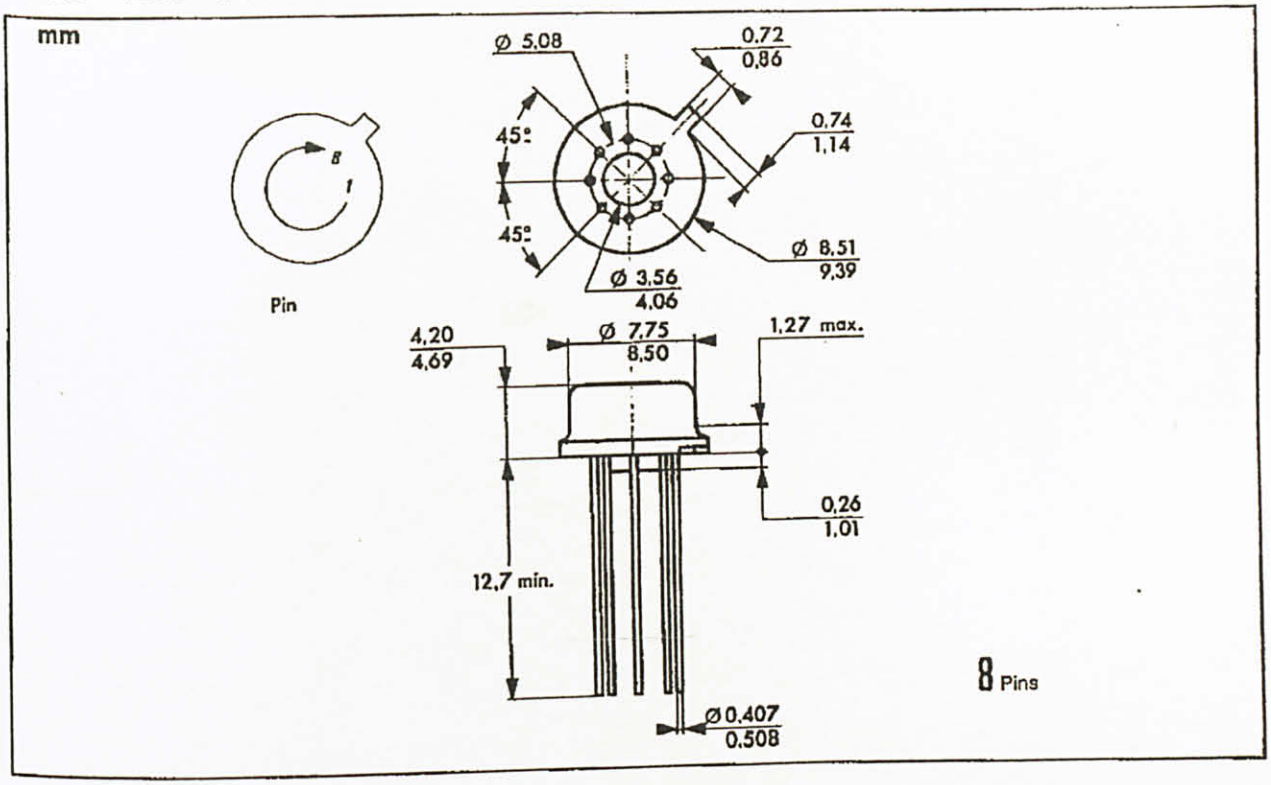

14 PINS – PLASTIC DIP

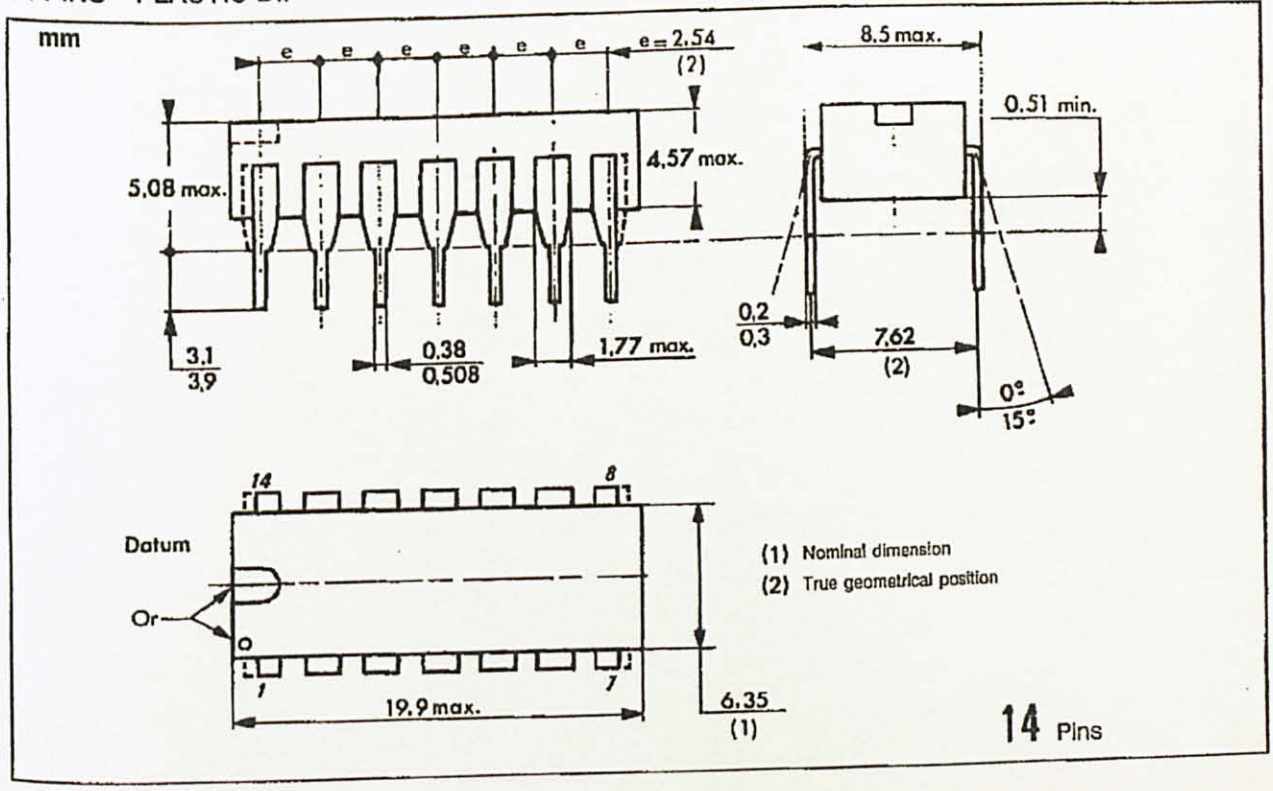

PACKAGE MECHANICAL DATA (continued)

8 PINS – PLASTIC DIP OR CERDIP

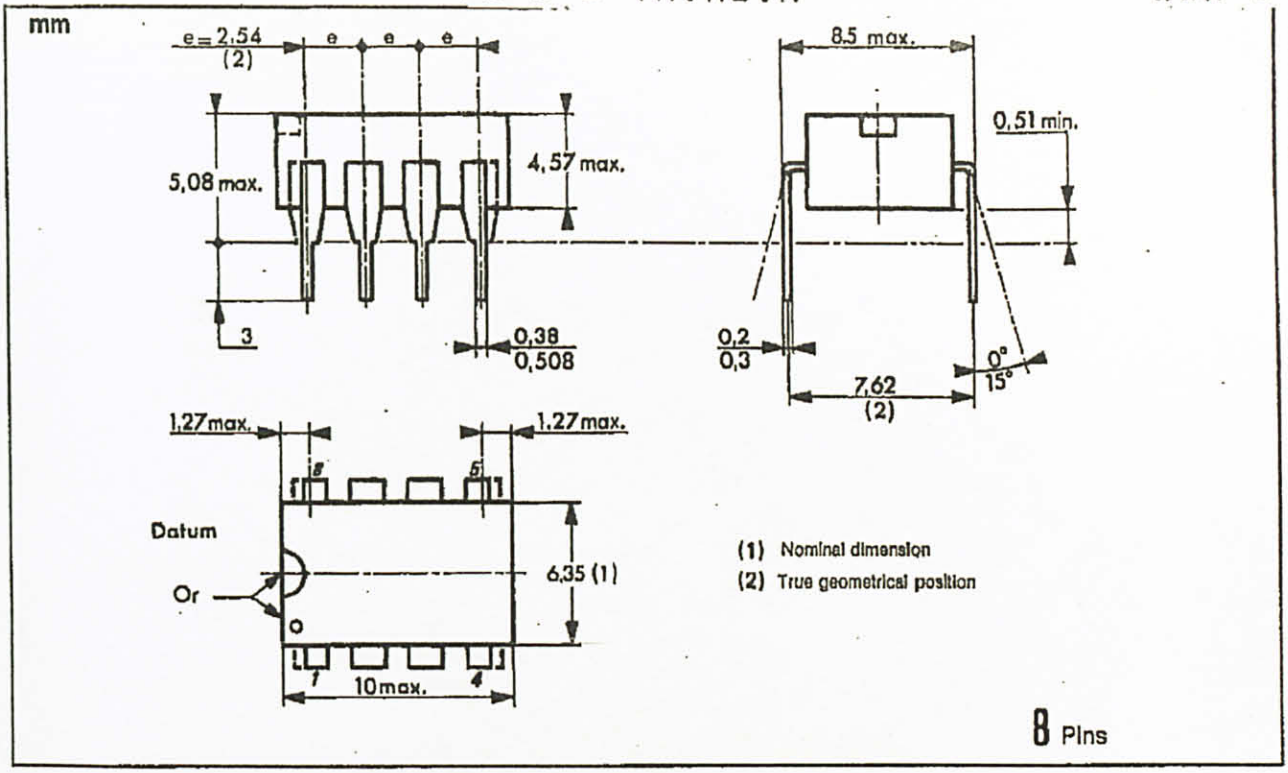

20 PINS – TRICECOP (LCC)

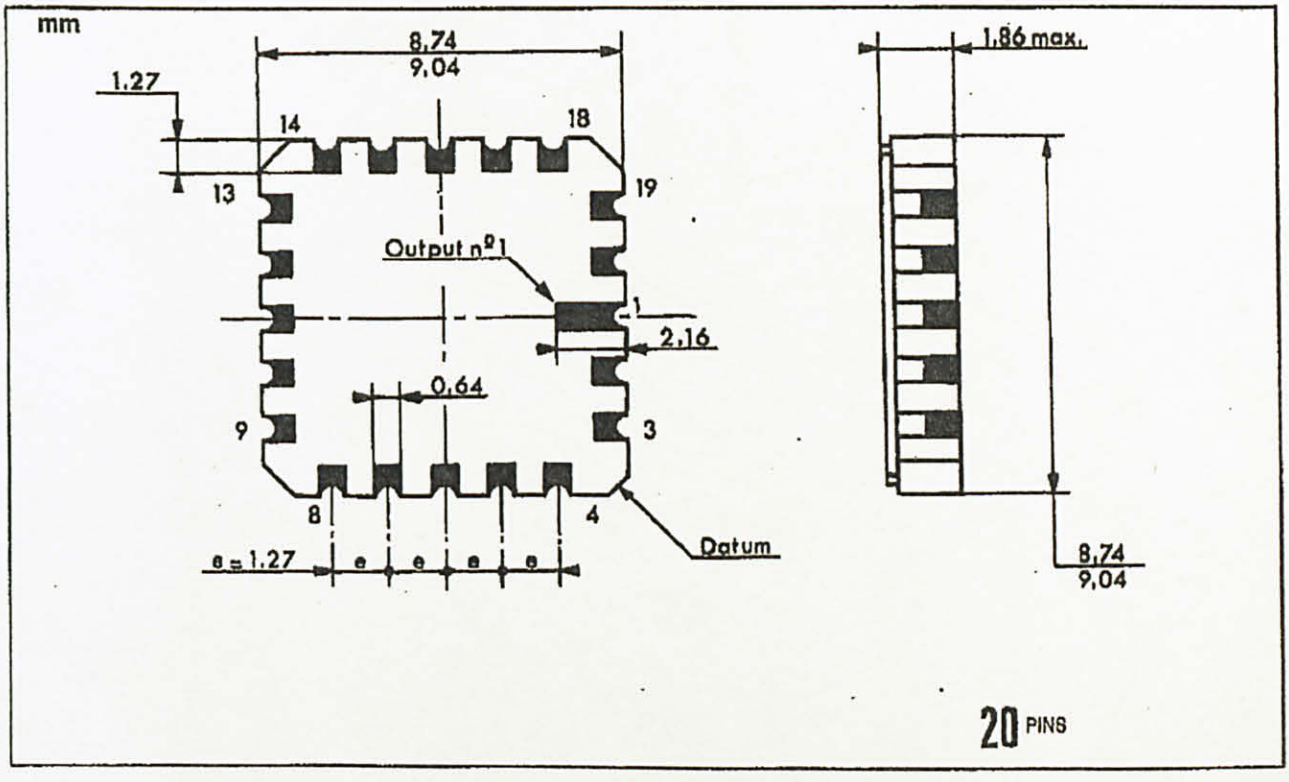

PACKAGE MECHANICAL DATA (continued)

8 PINS – PLASTIC MICROPACKAGE (SO) S G S-THOMSON 30E D

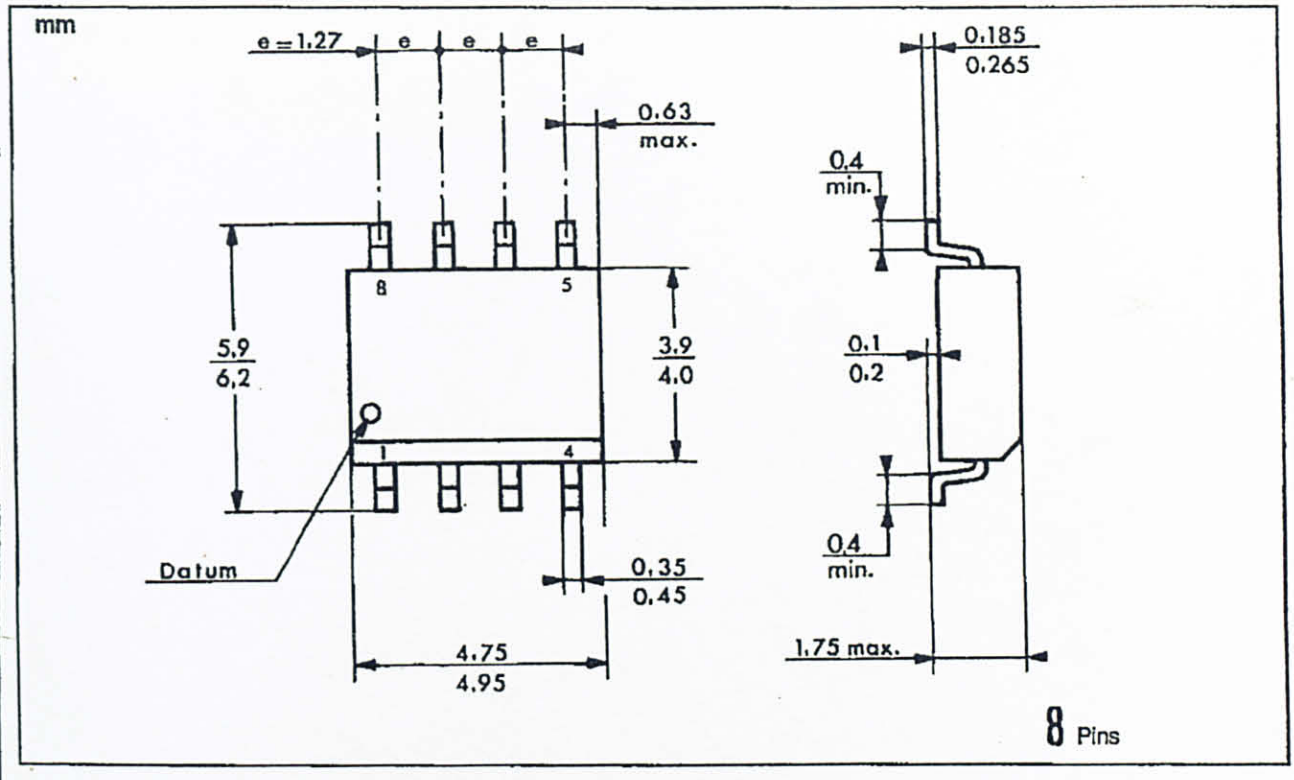

PACKAGE MECHANICAL DATA (continued)

8 PINS – PLASTIC MICROPACKAGE (SO) S G S-THOMSON 30E D

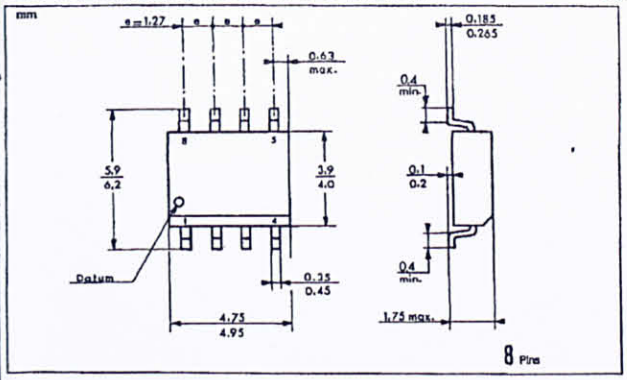

APPENDIX C

TOROID INFORMATION SHEET

Type : T Cores

Ordering Code:

P4 T5.84*3.05*1.52 HP G□

Material 材質 | Core Size 品名 | Coating 塗裝 | Gapped AL Value

C : Epoxy Coating of Halogen-Free
HP : Parylene Coating of Halogen-Free
UC : Epoxy Coating of UL & Halogen
P : Parylene Coating of Halogen

Shape:

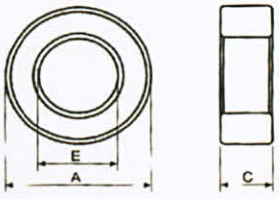

■ DIMENSIONS AND EFFECTIVE PARAMETERS

CORES	DIMENSIONS (mm) PARYLENE COATING DIMENSIONS (mm) A	E	C	EFFECTIVE PARAMETERS C1(mm-1)	Le(mm)	Ae(mm²)	Ve(mm³)	Wt(g/set)
T5.84x3.05x1.52	5.84 ± 0.15 5.84 ± 0.15	3.05 ± 0.15 3.05 ± 0.15	1.52 ± 0.15 1.52 ± 0.15	6.59	13.96	2.12	29.61	0.142
T5.84x3.05x3.05	5.84 ± 0.15 5.84 ± 0.15	3.05 ± 0.15 3.05 ± 0.15	3.05 ± 0.15 3.05 ± 0.15	3.28	13.96	4.25	59.41	0.296
T5.95x2.8x2.5	5.95 ± 0.30 5.95 ± 0.30	2.80 ± 0.30 2.80 ± 0.30	2.50 ± 0.20 2.50 ± 0.20	3.49	13.74	3.94	54.12	0.262
T6x3x2	6.00 ± 0.30 6.00 ± 0.30	3.00 ± 0.30 3.00 ± 0.30	2.00 ± 0.20 2.00 ± 0.20	4.71	14.14	3.00	42.41	0.21
T6x3x3	6.00 ± 0.30 6.00 ± 0.30	3.00 ± 0.30 3.00 ± 0.30	3.00 ± 0.20 3.00 ± 0.20	3.14	14.14	4.50	63.62	0.32
T6x4x2.15	6.00 ± 0.30 6.00 ± 0.30	4.00 ± 0.30 4.00 ± 0.30	2.15 ± 0.20 2.15 ± 0.20	7.31	15.71	2.15	33.70	0.17
T6.22x2.8x3.38	6.22 ± 0.30 6.22 ± 0.30	2.80 ± 0.30 2.80 ± 0.30	3.38 ± 0.20 3.38 ± 0.20	2.45	14.16	5.77	81.85	0.40
T6.35x3.81x3.18	6.35 ± 0.30 6.35 ± 0.30	3.81 ± 0.30 3.81 ± 0.30	3.18 ± 0.20 3.18 ± 0.20	3.95	15.96	4.04	64.45	0.30
T6.5x3.5x2.3	6.50 ± 0.30 6.50 ± 0.30	3.50 ± 0.25 3.50 ± 0.25	2.30 ± 0.20 2.30 ± 0.20	4.55	15.70	3.45	54.17	0.27
T7.1x4.4x2.7	7.10 ± 0.30 7.10 ± 0.30	4.40 ± 0.30 4.40 ± 0.30	2.70 ± 0.30 2.70 ± 0.30	1.35	18.06	3.65	66.00	0.62
T7.62x3.18x4.8	7.62 ± 0.15 7.62 ± 0.15	3.18 ± 0.15 3.18 ± 0.15	4.80 ± 0.15 4.80 ± 0.15	1.59	16.96	10.66	180.77	0.89
T8x4x2	8.00 ± 0.30 8.00 ± 0.30	4.00 ± 0.20 4.00 ± 0.20	2.00 ± 0.20 2.00 ± 0.20	4.71	18.85	4.00	75.40	0.37
T8x4x4	8.00 ± 0.30 8.00 ± 0.30	4.00 ± 0.20 4.00 ± 0.20	4.00 ± 0.30 4.00 ± 0.30	2.36	18.85	8.00	150.80	0.76
T8x4.5x4	8.00 ± 0.30 8.00 ± 0.30	4.50 ± 0.20 4.50 ± 0.20	4.00 ± 0.30 4.00 ± 0.30	2.80	19.63	7.00	137.44	0.65
T8.15x4.3x4.05	8.15 ± 0.30 8.15 ± 0.30	4.30 ± 0.30 4.30 ± 0.30	4.05 ± 0.30 4.05 ± 0.30	2.51	19.56	7.80	152.47	0.75
T8.35x3.33x4.18	8.35 ± 0.30 8.35 ± 0.30	3.33 ± 0.20 3.33 ± 0.20	4.18 ± 0.20 4.18 ± 0.20	1.74	18.33	10.49	192.39	0.93
T8.89x3.81x4.83	8.89 ± 0.15 8.89 ± 0.15	3.81 ± 0.15 3.81 ± 0.15	4.83 ± 0.15 4.83 ± 0.15	1.62	19.39	12.26	244.61	1.16

Appendix c continued.....

MANUFACTURING CAPABILITY

Gapped Toroid Sizes(OD)	2.50mm - 12.00mm
Height	0.70mm - 8.00mm
Gap Sizes :	0.03mm - 0.80mm
AL Tolerance	AL ± 10%

APPLICATIONS

Power
- DC-DC Converters
- Compact Power Transformer
- Small, Low Profile Power Inductors

Telecom
- xDSL pass-band Filiters
- Spilters
- EMI Inductors
- Filiter Inductors with Tight Tolerance

■ ELECTRICAL CHARACTERISTICS

	AL ± 25% (nH/N²)							AL ± 30% (nH/N²)			
CORES	P4	P5	N42	S3	A043	A05	A07	A10	A102	A121	A151
T5.84x3.05x1.52	490		725		860	980	1370	1960	1960		2860
T5.84x3.05x3.05	990	765			1720	1980	2770	3960	3960	4600	5750
T5.95x2.8x2.5										4320	5400
T6x3x2	660	530			1200	1450	2200	2600	2600	3200	4000
T6x3x3	1000	800	1520		1800	2200	2800	4000	4000	4800	6000
T6x4x2.15	430	340			700	870	1200	1740	1740	2080	
T6.22x2.8x3.38	1280		1950			2560		5130	5130		
T6.35x3.81x3.18	790	630	1210			1590	2220	3180	3180	3820	
T6.5x3.5x2.3	690					1380	1930				4140
T7.1x4.4x2.7					970						
T7.62x3.18x4.8	2090		3000			4175	5845	8350	8350	9480	11850
T8x4x2	660	550			1200	1330	1870	2670	2670	3200	4000
T8x4x4	1300		2030		2400	2650	3700	5300	5300	6400	8000
T8x4.5x4	1100	900				2200	3100	4450	4450	5380	6725
T8.15x4.3x4.05	620							5010	5010	6015	7520
T8.35x3.33x4.18			2730				5030			8625	10790
T8.89x3.81x4.83	1930										11600

Remark:
1. AL Value Testing Condition : 10kHz, 50mV, 1Ts. If testing condition is different from ACME's, please specify upon request & ordering.
2. Coating Material
(1) Toroid Size T8 and Below:clear parylene coating, breakdown voltage:1000Vdc, coating thickness : 0.05mm max.
(2) Toroid Size T9 and Above:green epoxy coating, breakdown voltage:1500Vdc, coating thickness : 0.6mm max.

APPENDIX D

PROJECT MILE STONES

Milestones for the Fyp 1

No.	Detail/ Week	1	2	3	4	5	6	7		8	9	10	11	12	13	14
1	Selection of Project Topic	■	■						Mid-semester break							
2	Preliminary Research Work		■	■	■											
3	Submission of Preliminary Report				●											
4	Seminar 1					■	■	■								
5	Project Work					■	■	■								
6	Submission of Progress Report									●						
7	Seminar 2										■	■	■	■		
8	Project work continues									■	■	■	■	■		
9	Submission of Interim Report Final Draft														●	
10	Oral Presentation															●

● Milestone

■ Process

APPENDIX D1

Milestones for Fyp II

No.	Detail/ Week	1	2	3	4	5	6	7		8	9	10	11	12	13	14
1	Project Work Continue	■	■	■												
2	Submission of Progress Report 1			●												
3	Project Work Continue				■	■	■	■								
4	Submission of Progress Report 2								●							
5	Seminar										■	■	■			
5	Project work continue								■	■	■	■	■			
6	Poster Exhibition										●					
7	Submission of Dissertation														●	
8	Oral Presentation															
9	Submission of Project Dissertation (Hard Bound)															●

Mid-Semester Break

● Milestone

■ Process

APPENDIX D2